

Ln[DO3A-*N*- α -(pyrenebutanamido)propionate] complexes: optimized relaxivity and NIR optical properties

M.F. Ferreira^a, G. Pereira^a, A.F. Martins^{b,c}, C.I.O. Martins^b, M.I.M. Prata^d, S. Petoud^c, E. Toth^c, P.M.T. Ferreira^a, J.A. Martins^{a,e*}, C.F.G.C. Geraldes^b

^aCentro de Química, Campus de Gualtar, Universidade do Minho, 4710-057 Braga, Portugal;

^bDepartment of Life Sciences, Faculty of Science and Technology, Centre of Neurosciences and Cell Biology, and Coimbra Chemistry Centre, University of Coimbra, 3001-401 Coimbra, Portugal;

^cCentre de Biophysique Moléculaire CNRS, Rue Charles Sadron, 45071 Orléans Cedex 2 France ;

^dICNAS and IBILI, Faculty of Medicine, University of Coimbra, 3000-548 Coimbra, Portugal;

^eCurrently in sabbatical leave at the Dep. Of Chemistry University of Bath, UK;

Corresponding author: José A. Martins, Centro de Química, Campus de Gualtar, Universidade do Minho, 4710-057 Braga, Portugal.

Abstract

We have proposed recently that the DO3A-*N*- α -(amino)propionate chelator and its amide conjugates are leads to targeted, high relaxivity, safe Contrast Agents for Magnetic Resonance Imaging. In this work we illustrate further the expeditious nature and robustness of the synthetic methodologies developed by preparing the DO3A-*N*-(α -pyrenebutanamido)propionate chelator. Its Gd³⁺ chelate retains the optimized water exchange, high stability and inertness of the parent complex. The pyrene moiety imparts concentration-dependent self-assembly properties and aggregation-sensitive fluorescence emission to the Gd³⁺ complex. The Gd³⁺ complex displays pyrene-centred fluorescence whilst the Yb³⁺ and Nd³⁺ complexes exhibit sensitized lanthanide-centred near-infrared luminescence. The aggregated form of the complex displays high relaxivity (32 mM⁻¹s⁻¹, 20 MHz, 25 °C) thanks to simultaneous optimization of the rotational correlation time and of the water exchange rate. The relaxivity is however still limited by chelate flexibility. This report demonstrates that the DO3A-*N*-(α -amino)propionate chelator is a valuable platform for constructing high relaxivity CA using simple design principles and robust chemistries accessible to most chemistry labs.

Introduction

Positron Emission Tomography (PET), Single Photon Emission Correlated Tomography (SPECT), Magnetic Resonance Imaging (MRI), Ultra Sound (US), and X-ray Computerized Axial Tomography (CAT), are imaging modalities used nowadays regularly in hospitals for diagnostic and prognostic purposes.¹ MRI has become in recent years the most useful imaging modality in the clinical setup. This results from its superb spatial resolution, use of non-ionizing radiation (radiofrequencies and magnetic fields), depth independent imaging and the possibility of repeated imaging to offset the low detection sensitivity of MRI which is intrinsic to the Nuclear Magnetic Resonance phenomenon. Signal intensity differences in MRI (contrast) arise mainly from intrinsic differences of the relaxation times ($T_{1,2}$) of the water protons of tissues. The contrast between normal and diseased tissues can be dramatically improved by paramagnetic Contrast Agents (CA) (Gd^{3+} , Mn^{2+} , stable nitroxide radicals, iron oxide nanoparticles, etc.), which shorten the relaxation times of the water protons.² Relaxivity ($r_{1,2}$), which is the paramagnetic enhancement of water proton relaxation rates $R_{1,2}$ ($R_{1,2} = 1/T_{1,2}$) normalized to 1 mM concentration, measures CA efficacy.^{2,3} The currently used CAs for T_1 -weighted MRI imaging are Gd^{3+} chelates of linear (DTPA-type) or macrocyclic (DOTA-type) poly(aminocarboxylate) chelators. Due to its long electronic relaxation times and high paramagnetism, Gd^{3+} efficiently enhances T_1 relaxation, resulting in signal intensity enhancement and bright images- positive contrast.⁴ High relaxivity CA can lead to T_1 reductions sufficient to generate effective contrast at low doses. Moreover, delivering CA to diseased areas can allow further dose reduction. Effective contrast at low CA doses (CA in clinical use are normally used at a dose of 0.1 mmol/Kg) became more important recently with the identification of the Nephrogenic Systemic Fibrosys (NSF) which is a debilitating and even deadly condition, associated to *in vivo* Gd^{3+} release from Gd-based CA.⁵ In fact, free (non-complexed) Gd^{3+} (and all other Ln^{3+} ions) are acutely toxic. Most NSF cases have been associated with the use of Gd^{3+} DTPA-type complexes, particularly $Gd(DTPA-bis-amide)$ CA.⁶ Low thermodynamic stability and kinetic lability, coupled to slow kidney clearance, results in extensive complex demetallation *in vivo*.⁷ Macrocyclic, DOTA-type Gd^{3+} complexes are generally considered safe given their higher thermodynamic stability and kinetic inertness.⁸ Chelates displaying simultaneous optimization of the molecular parameters that govern relaxivity, namely the rotational correlation time (τ_R), the water exchange rate ($k_{ex}=1/\tau_M$) and the electronic relaxation parameters, are expected to display very high relaxivities.⁹ There are well established strategies for tuning τ_R and k_{ex} into the optimal range to attain high relaxivities at intermediate fields relevant for clinical MRI. Tuning the Gd^{3+} ion electronic relaxation parameters turns out to be more challenging.¹⁰ Increasing the molecular

weight of chelates leads to longer rotational correlation times (τ_R) (slower tumbling rates) enhancing CA relaxivity at intermediate fields. Self-assembly of amphiphilic chelates into micelle-type supramolecular structures,¹¹ non-covalent association with Serum Albumin¹² and covalent attachment of chelates to macromolecular and nanoobjects (proteins,¹³ dendrimers,¹⁴ nanoparticles,¹⁵ viral capsules,¹⁶ quantum dots,¹⁷ etc.) are well established strategies to tune τ_R . Replacement of an ethylenediamine by a propylenediamine bridge or a pendant acetate by a propionate group on the DOTA and DTPA scaffolds enforces steric compression around the water binding site on Gd^{3+} complexes, leading to accelerated water exchange.^{11,18,19} A pendant propionate group leads to water exchange rate enhancements suitable for attaining high relaxivities at intermediate fields, without compromising the thermodynamic and kinetic stability of the chelates.^{18,20,21} Still, connecting linkers/spacers permit fast local rotational motions of the immobilized chelates superimposed to global slow rotational motions of the (entire) macromolecular object, resulting in suboptimal effective rotational correlation times.^{11,15}

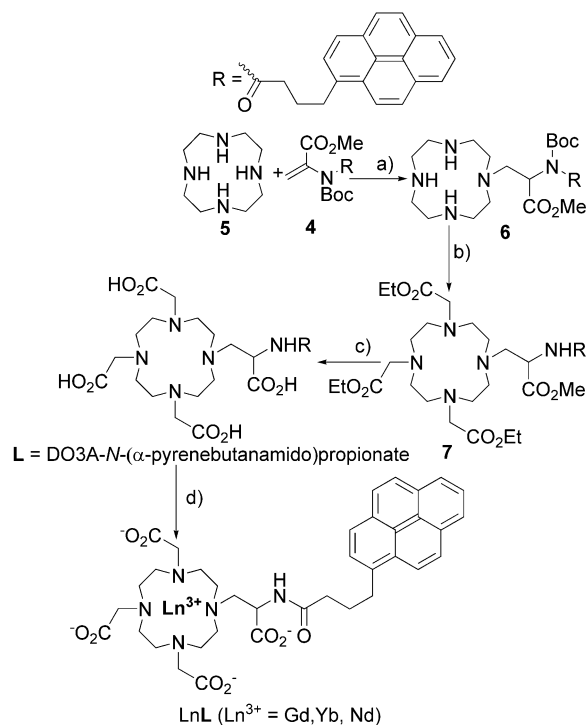
Endowing targeted high relaxivity Gd^{3+} chelates with fluorescence reporting capability results in bimodal MRI/fluorescence imaging agents. This approach has the potential to improve CA performance: the high detection sensitivity of fluorescence complements the low detection sensitivity of MRI, whilst the depth independent properties of MRI complement the limited light crossing into live tissues.²² Conjugates of metal chelate-fluorophores,²³ quantum dots^{17,24}, silica nanoparticles^{25,26} and other nanomaterials functionalised with Gd^{3+} chelates have been described as bimodal MRI/fluorescence imaging agents. The aggregation sensitive fluorescence properties of the pyrene fluorophore²⁷ make pyrene conjugates especially attractive as “responsive” probes for structural,²⁸ biochemical and cellular studies²⁹ and as chemical sensors.³⁰ Moreover, pyrene has been used as antenna for sensitizing near infrared (NIR) emitting Ln^{3+} ions (Yb^{3+} , Nd^{3+} and Er^{3+}) in DOTA and DTPA chelates.^{31,32}

We have recently described methodologies for the synthesis of the DO3A-*N*-(α -amino)propionate chelator and for preparing its amide conjugates.^{18,21} Gd^{3+} complexes of those amide conjugates retain the optimal water exchange, high stability and kinetic inertness of the parent complex.¹⁸ In this work we describe the synthesis of the pyrenebutyric acid conjugate of the DO3A-*N*-(α -amino)propionate chelator and its Ln^{3+} complexes. The effect of self-assembly on the relaxivity and fluorescence properties of the $Gd[DO3A-N-(\alpha$ -pyrenebutanamido)propionate] complex was studied by relaxometry and steady state fluorescence. The potential of the pyrene moiety to sensitize NIR emitting Ln^{3+} ions has been also addressed.

Results and Discussion

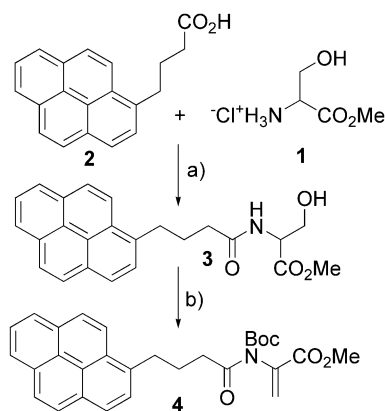
Synthesis

The DO3A-*N*-(α -pyrenebutanamido)propionate chelator (**L**) was synthesised following the (indirect) methodology proposed before for amide conjugates of the DO3A-*N*-(α -amino)propionate chelator (Scheme 1).²¹



Scheme 1. Synthetic pathway for the metal chelator DO3A-*N*-(α -pyrenebutanamido)propionate (**L**) and its Ln^{3+} complexes LnL : a) $\text{K}_2\text{CO}_3/\text{MeCN}$; b) i. TFA/DCM, ii. Ethyl bromoacetate, $\text{K}_2\text{CO}_3/\text{MeCN}$; c) i. Dowex 1X2-OH, ii. Elution with hydrochloric acid 0.1 M; d) $\text{LnCl}_3 \cdot x\text{H}_2\text{O}$.

The *N*-(α -pyrenebutanamido)propionate pendant group was introduced, early on the synthesis, into the *cyclen* scaffold *via* Michael addition of the dehydroalanine (Pyrene, Boc)- Δ -AlaOMe reactive block (**4**). Synthetic block (**4**) was prepared in 2 steps in 70% overall yield following the procedure developed by Ferreira and co-workers (Scheme 2).³³



Scheme 2. Synthesis of the dehydroalanine (Pyrene, Boc)- Δ -AlaOMe reactive block (**4**): a) i. TEA 2 molar equivalents/MeCN, ii. DCC/HOBt; b) Boc₂O, DMAP, dry MeCN.

After removing the *tert*-butyloxycarbonyl protecting group from the monoalkylated intermediate (**6**) with TFA, one pot *N*-alkylation of the *cyclen* scaffold with ethyl bromoacetate afforded prochelator **7**. Alkaline deprotection of **7** with Dowex1X2-OH⁻ resin, followed by resin elution with diluted hydrochloric acid afforded the DO3A-*N*-(α -pyrenebutanamido)propionate chelator (**L**) as hydrochloride in 30% overall yield over 3 steps. Recently, Caravan and co-workers have reported a similar pathway for the synthesis of conjugates of the DO3A-*N*-(α -amino)propionate chelator.³⁴ The synthesis of the DO3A-*N*-(α -pyrenebutanamido)propionate chelator further supports the use of the *indirect* pathway for amide conjugates of the DO3A-*N*-(α -amino)propionate chelator.

Relaxometric studies of the GdL complex

The concentration dependence of the paramagnetic water proton relaxation rate (R_{1p}) was evaluated for GdL (20 MHz, 25 °C, pH 7.0) in the concentration range 0.05-5.0 mM (**Figure 1**).

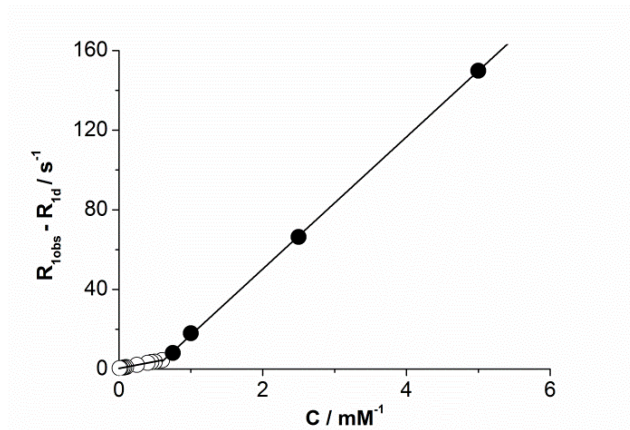


Figure 1. Concentration dependence of the paramagnetic water proton longitudinal relaxation rate $R_{1p} = (R_{1,obs} - R_{1,d})$ for GdL (20 MHz, 25 °C, pH 7.0).

The paramagnetic longitudinal relaxation rate data vs [GdL] define two straight lines with different slopes. This behaviour is characteristic of chelate self-assembly in aqueous solution, presumably into micelle-type structures, driven by the hydrophobic effect.¹¹ The break point gives an estimation of the critical micelle concentration, cmc (0.60 ± 0.02 mM), for GdL. Below the cmc , the complex is in a monomeric, non-aggregated, form in solution (Equation 1). Above the cmc , it is present in the form of aggregates as well as monomers whose concentration corresponds to the cmc (Equation 2).

$$R_{1p} = R_{1}^{obs} - R_{1}^d = r_1^{n.a} \times C_{Gd} \quad (1)$$

$$R_{1p} = R_{1}^{obs} - R_{1}^d = (r_1^{n.a} - r_1^a) \times cmc + r_1^a \times C_{Gd} \quad (2)$$

R_{1}^d is the diamagnetic contribution to the longitudinal relaxation rate (the relaxation rate of pure water), $r_1^{n.a}$ ($6.86 \pm 0.03 \text{ mM}^{-1} \text{ s}^{-1}$) represents the relaxivity of the free, non-aggregated Gd^{3+} chelate, r_1^a ($33.11 \pm 0.04 \text{ mM}^{-1} \text{ s}^{-1}$), is the relaxivity of the micellar (aggregated) form and C_{Gd} is the analytical Gd^{3+} concentration.

The micellar nature of GdL above the cmc (5.0 mM, pH 7.0) was confirmed by Dynamic Light Scattering (DLS) analysis (Figure S1). A bimodal intensity distribution, with the main population of particles displaying an average radius of 1.7 nm and a minor population exhibiting an average radius of 73 nm, was obtained by DLS, resulting in a population weighted mean hydrodynamic radius, expressed by the z-average parameter, of 49 nm. The temperature (**Figure S2**) and the pH dependence (**Figure S3**) of the paramagnetic water proton relaxation rate was studied at 20 MHz.

Transmetallation studies against Zn^{2+} ions were also performed to evaluate the kinetic inertness of the complex (**Figure S4**). The temperature dependence study strongly suggests that below 50 °C, the relaxivity is not limited by slow water exchange. The pH-dependence and the transmetallation studies indicate that the **GdL** complex, like its non-associating Gd[DO3A-*N*-(α -benzoylamido)propionate] analogue, is stable towards protonation-assisted demetallation and inert towards transmetallation with Zn^{2+} .²¹

^{17}O NMR and ^1H NMRD studies

The magnetic field dependence of the longitudinal water proton relaxivities (^1H NMRD profiles) of GdL was recorded at 25 °C and 37 °C in the frequency range 0.01 to 80 MHz and at concentrations below (Figure 3) and above (Figures 2c) the *cmc*.

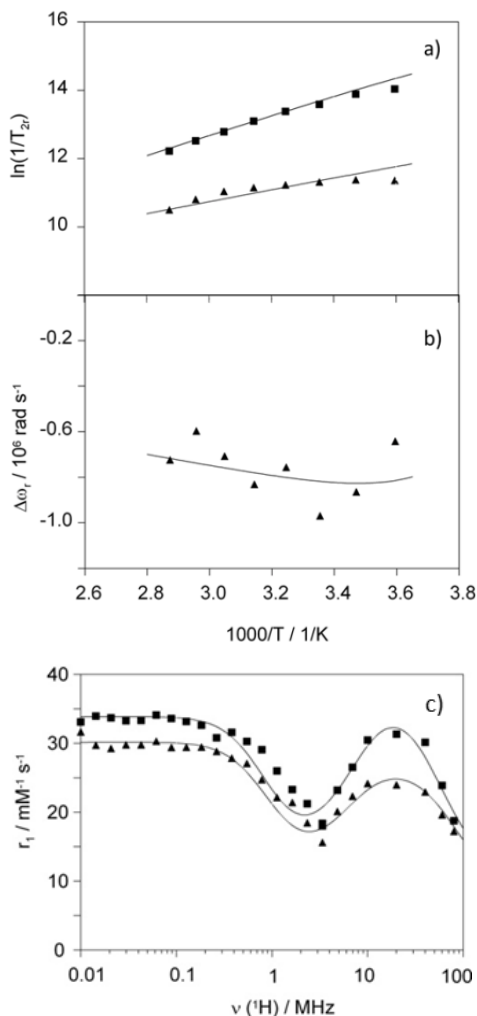


Figure 2. Temperature dependence of (a) reduced longitudinal, T_{1r} (■) and transverse, T_{2r} (▲) relaxation times and (b) chemical shifts ($\Delta\omega_r$) of a micellar aqueous solution of GdL at 11.7 T (5.0 mM, pH 7.0); (c) NMRD profiles of the aggregated micellar state (2.5 mM, pH 7.0) at 25 °C (■) and 37 °C (▲) after subtraction of the relaxation contribution of the monomer form. The curves represent results from the simultaneous fittings as described in the text.

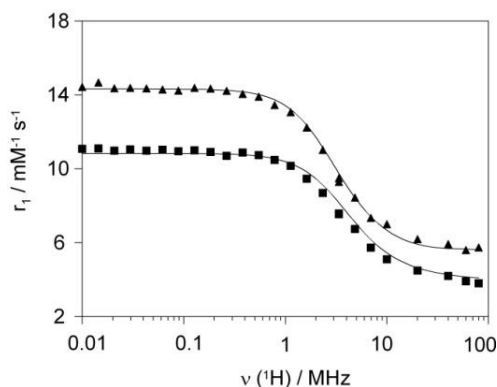


Figure 3. ^1H nuclear magnetic relaxation dispersion (NMRD) profiles of GdL in the monomer state at 0.3 mM at 25 °C (\blacktriangle) and 37 °C (\blacksquare). The curves represent results from the fittings as described in the text.

The NMRD curves are influenced by many parameters, the most important being the hydration number (q), the water exchange rate (k_{ex}), the electron relaxation parameters (τ_v and Δ^2) and the rotational correlation time (τ_R). The NMRD measurements have been completed with ^{17}O NMR data (**Figure 2a,b**). Indeed, from variable temperature ^{17}O T_2 measurements, one can accurately determine the water exchange rate. The rotational correlation time can be assessed by variable temperature ^{17}O T_1 measurements. On the other hand, variable temperature measurements of the chemical shift difference between bulk and bound water ($\Delta\omega_r$), give an indication of the q value.

The proton relaxation rates measured above the *cmc* represent the sum of the relaxivity contribution of the monomer complex, present at a concentration equal to the *cmc*, and the relaxivity contribution of the aggregated state. In order to calculate the relaxivity of the aggregated form, the relaxivity contribution of the monomer has been subtracted from the relaxation rates measured above the *cmc*. These profiles present the characteristic high field peak typical of slowly tumbling Gd^{3+} complexes. The ^{17}O NMR measurements have been performed at 5.0 mM concentration, largely above the *cmc* (0.6 mM). Under these conditions, one can consider that the rotational dynamics, as assessed by ^{17}O T_1 data, corresponds to the micellar state. Therefore, the ^{17}O NMR data have been fitted together with the NMRD curves of the micellar state to the Solomon-Bloembergen-Morgan theory by including the Lipari-Szabo treatment for the description of the rotational motion (**Table 1**).³⁵

Table 1. Best fit parameters obtained for the aggregated form of GdL from the simultaneous analysis of the ^{17}O NMR and ^1H NMRD data and for the monomer from NMRD data

Parameter	Aggregated form	Monomer
ΔH^\ddagger [kJmol $^{-1}$]	21.5 ± 1.5	<u>21.5</u>
k_{ex}^{298} [10^7 s $^{-1}$]	6.2 ± 0.5	<u>6.2</u>
τ_g^{298} [ps]	3780 ± 100	116 ± 5
τ_{IO}^{298} [ps]	930 ± 50	-----
S^2	0.24 ± 0.02	-----
$\tau_{\text{IH}}^{298}/\tau_{\text{IO}}^{298}$	0.80 ± 0.05	-----
E_g [kJmol $^{-1}$]	25.4 ± 0.7	-----
E_i [kJmol $^{-1}$]	12 ± 1	24.3 ± 0.2
Δ^2 [10^{20} s $^{-1}$]	0.033 ± 0.004	0.38 ± 0.04
τ_v^{298} [ps]	53 ± 5	6.3 ± 0.5
A/\hbar [10^6 rads $^{-1}$]	-3.2 ± 0.4	-----

Parameters underlined have been fixed;
 τ_{RO}^{298} values from ^{17}O T_1 data.

In this approach, two kinds of motion are assumed to modulate the interaction causing the relaxation, namely a rapid, local motion which lies in the extreme narrowing limit and a slower, global motion.

We calculate therefore τ_g , the correlation time for the global motion (common to the whole micelle), and τ_i , the correlation time for the fast local motion, which is specific for the individual relaxation axis, and thus related to the motion of the individual Gd^{3+} chelate units. The generalized order parameter, S , is a model-independent measure of the degree of spatial restriction of the local motion, with $S = 0$ if the internal motion is isotropic and $S = 1$ if the motion is completely restricted.

It was assumed that the GdL complex has one inner sphere water molecule ($q = 1$) like the low molecular weight amide analogue $\text{Gd}[\text{DO}_3\text{A}-N-(\alpha\text{-benzoylamido})\text{propionate}]^{21}$ and the parent amine $\text{Gd}[\text{DO}_3\text{A}-N-(\alpha\text{-amino})\text{propionate}]^{18}$. This assumption was confirmed by the value obtained for the scalar coupling parameter ($A/\hbar = -3.2 \times 10^6$ rad s $^{-1}$).³⁶

The NMRD curves of the monomer sample (0.3 mM) have been analyzed by fixing the water exchange parameters (k_{ex}^{298} , ΔH^\ddagger) to those obtained from the ^{17}O NMR data. In the fits, we have fixed the r_{GdH} distance to 3.10 Å and the distance of closest approach of the bulk water protons to the Gd^{3+} , a_{GdH} , to 3.65 Å. The diffusion constant has been fixed to 23×10^{-10} m 2 /s and its activation energy to 20 kJ/mol.

The NMRD profile for the monomeric form is characteristic of low molecular weight complexes (**Figure 3**). The relaxivity at intermediate field ($5.9 \text{ mM}^{-1} \text{ s}^{-1}$; $25 \text{ }^\circ\text{C}$, 20 MHz) is dominated by fast rotation in solution as indicated by the short τ_R value obtained (116 ps). In contrast, above the *cmc* the NMRD profile of GdL displays a hump at intermediate field, typical of slow tumbling species (**Figure 2c**).^{11,15,35}

The relaxivity decreases with increasing temperature, indicating that it is not limited by slow water exchange. The same behaviour was previously observed for gold nanoparticles functionalised with the analogous cysteine conjugate Gd[DO₃A-*N*-(α -cystamido)propionate].¹⁵ The water exchange rate on GdL is similar to that reported for the low molecular weight amide analogue Gd[DO₃A-*N*-(α -benzoylamido)propionate]²¹ and slightly higher than that reported for the parent Gd[DO₃A-*N*-(α -amino)propionate]¹⁸ complex ($k_{ex}^{298}/10^7 = 6.2, 5.7$ and 4.0 s^{-1} , respectively). This value is in the ideal range for attaining high relaxivities at intermediate magnetic fields relevant for clinical applications.¹⁹ The Lipari-Szabo analysis of the longitudinal ¹H and ¹⁷O relaxation rates allows separating fast local rotational motions of the chelate ($\tau_{Rl} = 930 \text{ ps}$) from the global rotational correlation time ($\tau_{Rg} = 3780 \text{ ps}$) of the micellar aggregate.

The value of the order parameter for GdL ($S^2 = 0.24$) is similar to those calculated for amphiphilic DOTA-type complexes functionalised with hexadecyl alkyl chains: Gd(DOTASAC18)³⁷ and Gd(DOTAMAP-En-C18)³⁸ ($S^2 = 0.24$ and 0.28 , respectively) (**Figure 4** and **Table 2**).

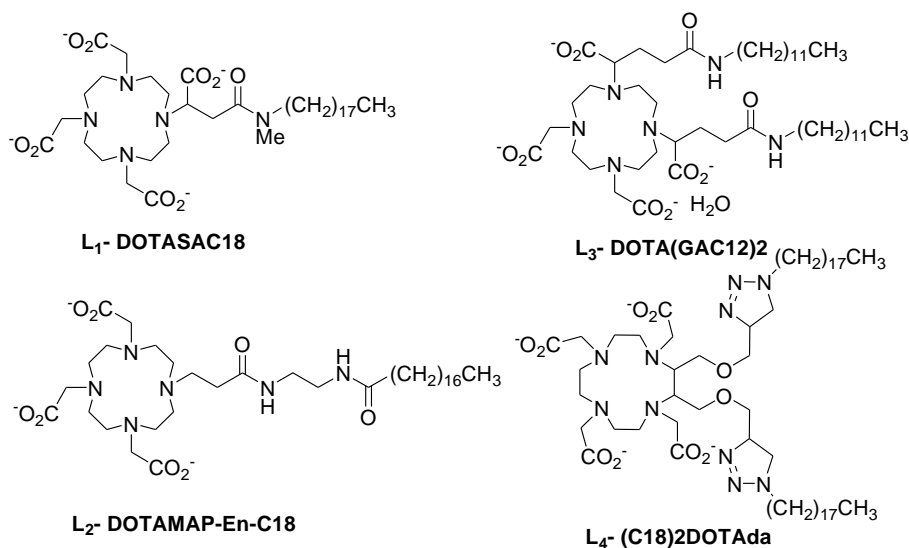


Figure 4. Structure of amphiphilic DOTA-type ligands compared in Table 2 and discussed in the text.

Table 2. Molecular parameters for amphiphilic DOTA-type complexes

Chelate	MW (g/mol)	<i>cmc</i> (mM)	τ_l^{298} (ps)	τ_g^{298} (ps)	S^2	k_{ex}^{298} (/10 ⁷ s ⁻¹)	$r_1^{m,f}$ (mM ⁻¹ s ⁻¹)
GdL ^a	881.2	0.06	330	2810	0.28	0.48	20.7
GdL ^b	881.2	-	271	2696	0.21	8.12	24.2
GdL ^c	1036	<0.1	820	4700	0.70	0.34	34.8
GdL ^d	1285	0.004	135	5206	0.78	0.30	35
GdL ^e	857	0.6	930	3780	0.24	6.2	32.2

^aref.37; ^bref. 38; ^cref.40; ^dref.39; ^ethis work; ^f(20MHz, 25°C)

Complexes functionalised with two long alkyl chains, Gd[(C18)₂DOTAda]³⁹ and Gd[(DOTA(GAC₁₂)₂)]⁴⁰, are characterised by substantially higher order parameters ($S^2 = 0.78$ and 0.70 , respectively). Tighter packing of the monomers and double anchoring through adjacent sites into the micelle structure restrict internal rotational movements of the chelates.

Moreover, the complex Gd[(C18)₂DOTAda] functionalised with two alkyl chains displays a much lower *cmc* value than the complex Gd(DOTASAC18) functionalised with one alkyl chain. In this respect, the GdL complex displays a relatively high *cmc* value (0.6 vs 0.06 and 0.004 mM for Gd[(C18)₂DOTAda] and Gd(DOTASAC18), respectively) reflecting probably the aromatic nature of the pyrene lipophylic moiety and the deviation of the overall shape of the conjugate from the wedge-like geometry which would be ideal for micelle formation.

The relaxivity displayed by the micellar form of GdL (32 mM⁻¹s⁻¹, 20 MHz, 25 °C) is substantially higher than that shown by the Gd(DOTASAC18) and Gd(DOTAMAP-En-C18) complexes (24.2 and 20.7 mM⁻¹s⁻¹, respectively) and it is similar to the relaxivity of the double chain chelates Gd[(C18)₂DOTAda] and Gd[(DOTA(GAC₁₂)₂)] (35 and 34.8 mM⁻¹s⁻¹, respectively). The high relaxivity of the double chain chelates has been ascribed to restricted local motions of the complex ($S^2 = 0.78$) and to the slow global rotational motion (τ_g). Importantly, GdL displays a relaxivity similar to that of the double chain chelates, despite a lower global rotational correlation time ($\tau_g = 3780$ vs 5206 and 4700 ps for Gd[(C18)₂DOTAda] and Gd[(DOTA(GAC₁₂)₂)], respectively) and a substantially lower degree of coupling of global and local rotational motions (higher flexibility) ($S^2 = 0.24$ vs 0.78 and 0.70 for Gd[(C18)₂DOTAda] and Gd[(DOTA(GAC₁₂)₂)], respectively). Importantly, the relaxivity of the double chain chelates is limited by slow water exchange ($k_{ex}^{298}/10^7 = 6.2$ vs 0.30 and 0.34 s⁻¹ for GdL and Gd[(C18)₂DOTAda] and Gd[(DOTA(GAC₁₂)₂)], respectively).

The high relaxivity attained by GdL can be thus ascribed to simultaneous optimization of τ_R and k_{ex} . The optimization of the rotational dynamics of complexes has been firmly established for relaxivity enhancement at intermediate fields. The simultaneous optimization of τ_R and k_{ex} is far more demanding and often achieved at the expense of complex stability compromising potential biological applications. This study highlights the importance of simultaneous optimization of all molecular parameters in order to attain high relaxivities and provides further support for our claim that amide conjugates of the DO3A-*N*- α -aminopropionate chelator are valuable synthons for constructing high relaxivity safe CA for MRI.

Luminescence studies

The Gd[(DO₃A-*N*-(α -pyrenebutanamido)propionate)] complex was designed as a bimodal MRI/fluorescence probe. The pyrene fluorophore was selected to impart self-assembly properties and concentration-dependent fluorescence reporting capability to the paramagnetic complex.²⁷

The absorption (**Figure S6**) and the fluorescence emission properties (**Figure S7**) of the free ligand **L** and the Gd**L** complex were studied in non-deoxygenated water (pH 7.0) at concentrations well below the *cmc* by UV-Vis and steady-state fluorescence spectroscopy (Table 3).

Table 3 - Maximum absorption (λ_{abs}) and emission wavelengths (λ_{em}), molar extinction coefficients (ϵ) and fluorescence quantum yields (Φ_{F}) for ligand **L** and Gd**L** complex (λ_{ex} 345 nm) in non-deoxygenated water at concentrations below the *cmc*.

$\lambda_{\text{abs}}(\text{nm})$ ($\epsilon/10^4 \text{ M}^{-1}\text{cm}^{-1}$) ^b		$\lambda_{\text{em}}(\text{nm})$		$\Phi_{\text{F}}^{a,c}$	
L	GdL	L	GdL	L	GdL
344 (3.26)	344 (4.43)				
328 (2.35)	328 (3.20)				
314 (1.00)	314 (1.59)	377	377		
277 (3.60)	277 (5.59)	397	398	0.22	0.17
266 (2.05)	266 (3.78)	417	418		
243 (5.62)	243 (9.19)				

^aRelative to anthracene in ethanol ($\Phi = 0.27$)
^bLigand and complex at 1×10^{-5} M concentration
^cLigand and complex at 1×10^{-6} M concentration, non-deoxygenated solutions

At concentrations below the *cmc* (*cmc* = 2.7 mM for **L**, see below, and 0.6 mM for Gd**L**), **L** and Gd**L** display similar absorption spectra in the region characteristic of pyrene (300-350 nm) assigned to intraligand $\pi-\pi^*$ transitions.³² Selective irradiation of the pyrene chromophore on **L** and Gd**L** at 345 nm yields fluorescence spectra displaying vibronically structured features, assigned to intraligand $^1\pi-\pi^*$ transitions, characteristic of pyrene monomer emission (Figure S5).^{32,41} At the concentration studied (well below the *cmc*) no excimer emission (broad featureless band with an emission with an apparent maximum located at 490-500 nm) was observed for both the free ligand and the Gd³⁺ complex. The fluorescence quantum yields for **L** and for the pyrene-centred emission in Gd**L** are of the same order of magnitude as those reported for other pyrene conjugates.

Complex formation with paramagnetic Gd³⁺ seems to have only a minor effect on the fluorescence quantum yield of **L**.⁴¹

We envisaged that it could be possible to monitor the self-assembly process of **L** and Gd**L** by taking advantage of the aggregation-sensitive fluorescence properties of the pyrenyl moiety.²⁷ With this aim, we studied by steady-state fluorescence the effect of the concentration on the fluorescence properties of **L** (**Figure S7**) and Gd**L** (**Figure 5**).

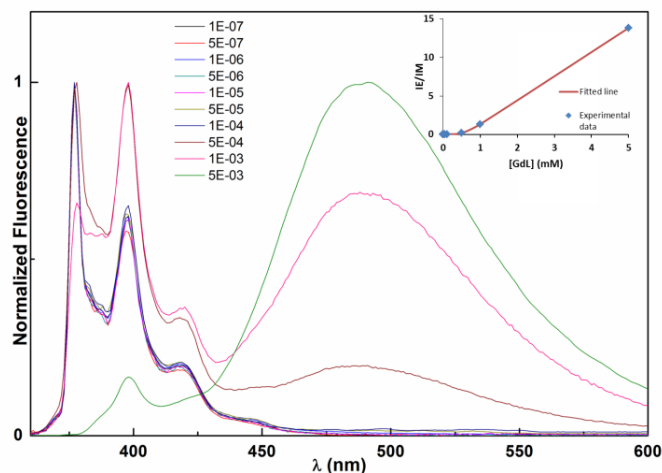


Figure 5. Normalized fluorescence spectra for Gd**L** in non-deoxygenated water over the concentration range 1×10^{-7} - 5×10^{-3} M ($\lambda_{\text{exc}} = 345$ nm). Inset- changes in the emission properties of Gd**L** as ratio of the fluorescence emission intensity for the *excimer* (I_E , 490 nm) and for the monomer (I_M , 377 nm) (I_E/I_M) as a function of Gd**L** concentration.

For low micromolar concentrations of **L** and Gd**L**, the fluorescence spectra display the characteristic vibronically structured pyrene monomer emission band. For higher (low millimolar) concentrations, the intensity of the monomer emission band is reduced and a new broad, red-shifted, featureless band, assigned to *excimer* formation, appears. The concentration dependence of the ratio of fluorescence emission intensity for the *excimer* (490 nm) and for the monomer (377 nm) (I_E/I_M) was used to determine independently the *cmc* for **L** (**Figure S7**) and Gd**L** (**Figure 5**) by fitting the experimental data points to a sigmoidal curve model (**Table S1**).^{42,43} A *cmc* value of approximately 0.64 mM, in excellent agreement with the value determined by relaxometry (0.60 mM), was derived for Gd**L** from the fluorescence study (**Figure 5**). A much higher *cmc* value (2.7 mM) was determined for the free ligand (**Figure S7**), reflecting the ionization state (multi-charged) of the free metal chelator. Below the *cmc*, the ligand and complex are molecularly dissolved and the fluorescence arises from the decay of excited monomers. Above the *cmc*, fluorescence emission arises predominantly from the decay of excited dimers- *excimers*. Higher concentrations of Gd**L** increase the number of micelles and enhance *excimer* formation and the corresponding fluorescence emission intensity. Two different mechanisms have been established for *excimer* emission: diffusive encounter of an excited monomer with a ground state molecule and the direct excitation of (pre-associated) ground state dimers. The partitioning of the

different modes of *excimer* formation depends on the fluidity of the micelle environment. Time-resolved fluorescence experiments suggest that the diffusive mechanism is the main contributor to *excimer* formation in cationic *gemini* surfactants containing a pyrene moiety and a long alkyl chain.⁴⁴ The order parameter determined for the micellar form of GdL ($S^2 = 0.24$) indicates that the micelles are fluid, suggesting that the diffusive mechanism might be responsible for *excimer* formation. Deciphering the mechanism of *excimer* formation in GdL micelles is outside the scope of the present study. The pyrene-centered fluorescence of GdL effectively provides this complex with MRI/fluorescence bimodal imaging agent activity. From the practical point of view, the pyrene centred fluorescence of GdL could be used for imaging studies in small animal models, for *ex vivo* characterization of tissue distribution, cell internalization and intracellular chelate localization and studies with cell lines.⁴⁵

Lanthanide centred fluorescence in the visible (Eu^{3+} and Tb^{3+}) and in the NIR region (Nd^{3+} , Yb^{3+}) are well suited for biological imaging: enhanced light penetration into biological tissues (especially in the NIR region); elimination of interference from tissue auto-fluorescence using time-gating techniques; long wavelength excitation, far into the visible region. Very low molar absorptivities (*f-f* transitions are forbidden by Laporte's and parity rules) make the direct excitation of Ln^{3+} ions impracticable. The formation of emissive Ln^{3+} excited states requires sensitization by sensitizing groups that absorb excitation light and transfer the resulting energy to the Ln^{3+} excited states (antenna effect), usually through ligand-centred triplet excited states.⁴⁶ In this study, we tested the possibility of using the pyrene chromophore to sensitize near infrared emitting Ln^{3+} ions in the corresponding LnL complexes (Ln= Nd and Yb) (**Figure 6**).

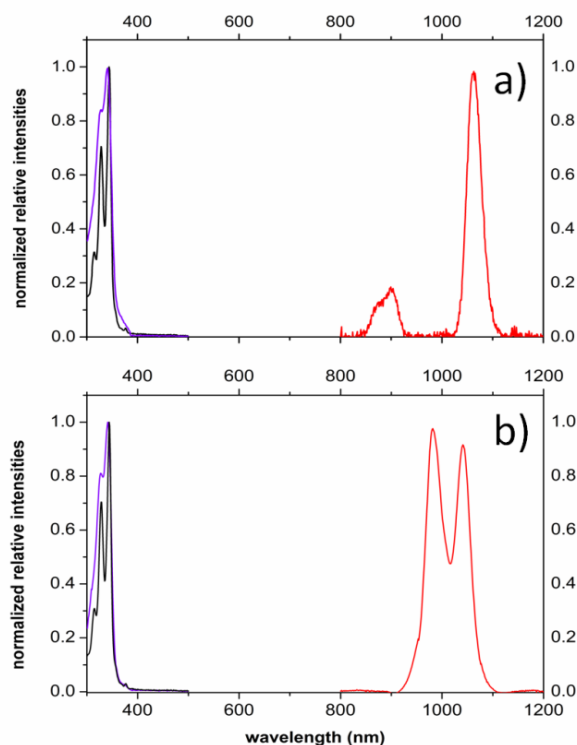


Figure 6. Absorbance (black), excitation ($\lambda_{\text{em}} = 1064$ nm, violet) and emission ($\lambda_{\text{exc}} = 344$ nm, red) spectra for the NdL complex (a), and YbL complex (b) in water.

Emission spectra of the NdL and YbL complexes under ligand excitation exhibit metal-centred NIR emission bands at ca 1064 nm (${}^4\text{F}_{3/2} \rightarrow {}^4\text{F}_{13/2}$) for NdL and a band with an apparent maximum at ca 1000 nm (${}^2\text{F}_{5/2} \rightarrow {}^2\text{F}_{7/2}$) for YbL.^{31,32} The excitation spectra for both luminescent Nd^{3+} and Yb^{3+} complexes are similar with each other and match well the profile of the corresponding absorption spectra as an indication that the sensitization of the lanthanide luminescence is occurring through the same electronic levels centred on pyrene.

Interaction of GdL with Human Serum Albumin (HSA)

The self-assembly of chelates into supramolecular structures (as discussed in this work) and binding to Serum Albumin (HSA) are robust strategies to enhance chelate relaxivity *via* optimization of τ_R . In addition to relaxivity enhancement, self-assembly and binding of chelates to HSA slow down CA leakage into the interstitial compartment, providing an extended time window for vasculature imaging (MRI angiography).⁴⁷ The binding affinity of GdL to HSA was assessed by Proton Relaxation Enhancement (PRE) measurements. The PRE methods are tailored to determine the differences in the NMR water solvent relaxation rates between protein-bound (resulting in an increase of the relaxation rates) and free substrates. Experimentally, it consists of measuring the water proton relaxation rates

$R_{1\text{obs}}$ in solution at increasing concentrations of the protein while keeping the concentration of the metal chelate constant (E-titration) or vice-versa (M-titration). The data obtained for the E-titration using a GdL concentration below the *cmc* (0.1 mM) and increasing HSA concentrations (**Figure 7**) were fitted to a one site binding model (**Equation S1**).

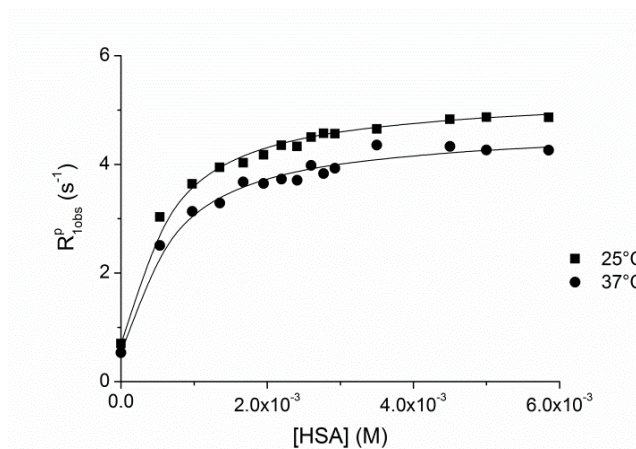


Figure 7. Proton Relaxation Enhancement data (20 MHz, pH 7.4) to assess HSA binding of GdL: E-titration at 0.1 mM GdL concentration at 25°C and 37°C.

The fitting affords an estimation of the relaxivity of the HSA-bound form, r_1^c (53.1 ± 6.7 and 47.0 ± 5.6 $\text{mM}^{-1}\text{s}^{-1}$ at 25 and 37 °C, respectively) and an apparent HSA-GdL association constant, K_A ($K_A = 1/K_d$) ($(1.9 \pm 0.1) \times 10^3$ and $(1.7 \pm 0.1) \times 10^3$ M^{-1} at 25 and 37 °C respectively). These values correspond to binding affinities similar to Gd(BOPTA)²⁻ but weaker than for MS-325, two blood pool agents presenting strong HSA binding.⁴⁸ In the limiting E-titration conditions ($[\text{GdL}] = 0.1$ mM and $[\text{HSA}] = 4\%$) the fraction of bound chelate can be estimated as higher than 90%. These values are in line with those reported recently by Caravan for similar amide conjugates.¹² It is known that HSA has multiple binding sites. Among the many studies published on HSA binding of Gd³⁺ complexes, typically those involving ultrafiltration experiments have reported binding to more than one independent sites with different binding constants.^{49,50} Those stepwise binding constants show that one binding site is much stronger than the others, justifying the common use a 1:1 binding isotherm to interpret the relaxometric data for albumin binding of Gd³⁺ complexes.⁵¹ In fact, most often relaxometric data alone do not allow for distinguishing between different binding models. An independent evaluation of K_A and n may be, in principle, pursued through the analysis of the data obtained from an M-titration, in which a fixed concentration of HSA is titrated with the Gd³⁺ complex. The titration of 4% HSA with GdL is restricted to the narrow range of concentrations below *cmc* precluding quantitative analysis of the data. The interaction of GdL with HSA is prone to modulate the biodistribution of GdL as recently reported for similar conjugates.^{12,52}

Biodistribution studies

The biodistribution profile of GdL was obtained after 1 and 24 hours post-injection (pi) using the $^{153}\text{Sm}^{3+}$ -labelled surrogate complex (Figure 8 and Table S2).

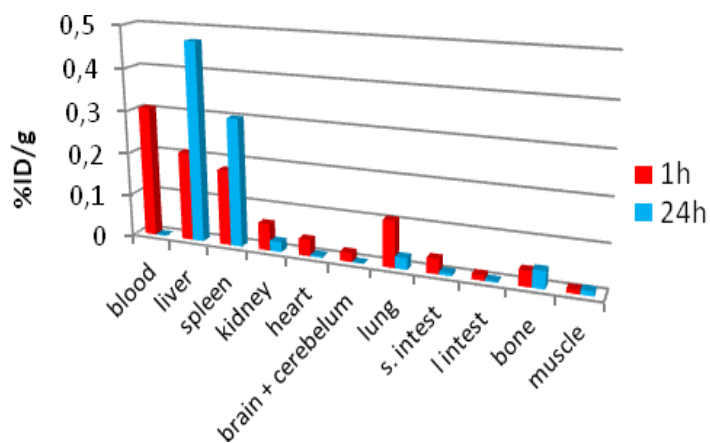


Figure 8. Biodistribution, stated as percentage of injected dose per gram of organ (%ID/g), of ^{153}SmL in Wistar rats 1 and 24 hours after *i.v.* injection. Results are the mean of 4 animals.

A recent Patent claims that peptides derivatised with pyrene are able to cross the blood-brain barrier thanks to (presumably) a correct lipophylicity/hydrophylicity balance imparted by the pyrene moiety.⁵³ This intriguing possibility was considered during the biodistribution study. The ^{153}SmL chelate displays biodistribution profiles at 1 and 24 hours pi similar to other micellar systems.⁵⁴ After 1 hour pi there is substantial activity in the blood, liver, spleen and lungs. The high activity in the blood after 1 hour pi reflects the micellar nature of the CA and its strong association with HSA, which slows down leakage of the complex into the interstitial compartment. The complex follows both hepatic and renal elimination. The hepatic and spleen uptake reflects the micellar nature of the CA and the role played by resident macrophages in the liver and spleen (Reticulo Endothelial System, RES) in clearing particulate material from the blood. The activity in the lungs might again reflect the retention of particulate material in narrow blood vessels and the extensive vascularisation of that organ and thus the high blood content of the lungs. The increase in activity in the spleen and liver after 24 hours pi correlates with the activity clearance from the blood and lungs, suggesting particle retention on those organs. Interestingly, after 1 hour pi, a low activity is measurable in the brain/cerebellum, suggesting that the complex might cross the blood-brain barrier. This possibility deserves further investigation.

Conclusions

The pyrenebutyric acid conjugate of the DO3A-*N*-(α -amino)propionate chelator was synthesised following synthetic methodologies reported previously by us. The lipophilic pyrene moiety imparts concentration-dependent self-assembly ability (presumably into micelles) to the Gd[DO₃A-*N*-(α -pyrenebutanamido)propionate] chelate. The aggregated form of the Gd³⁺ chelate displays high relaxivity thanks to simultaneous optimization of the rotational correlation time and of the water exchange rate. Nonetheless, the relaxivity is still limited by internal flexibility. The Gd³⁺ complex displays pyrene-centred fluorescence properties sensitive to its aggregation state. The Nd³⁺ and Yb³⁺ complexes exhibit lanthanide-centred sensitized NIR emission. The surrogate ¹⁵³Sm³⁺ complex displays a biodistribution profile similar to other micellar systems. Interesting applications of this probe can be based on the recent report that carbon-based nanomaterials (graphene, graphene oxide, carbon nanotubes) functionalized non-covalently with pyrene conjugates are promising for the development of exquisite probes for biological processes.⁵⁵ In summary, we have reported recently that Gd³⁺ complexes of amide conjugates of the DO3A-*N*-(α -amino)propionate chelator are new leads for targeted, high relaxivity, safe CA for in vivo MRI.²¹ In this work we provide further evidence to support this claim, using simple design principles and robust chemistry accessible to all laboratories.

Experimental

Materials and Methods

Chemicals were purchased from Sigma-Aldrich and used without further purification. Solvents used were of reagent grade and purified by usual methods. Cyclen was purchased from CheMatech, France. Reactions were monitored by TLC on Kieselgel 60 F254 (Merck) on aluminium support. Detection was by examination under UV light (254, 365 nm) and by adsorption of iodine vapour. Flash chromatography was performed on Kieselgel 60 (Merck, mesh 230-400). The relevant fractions from flash chromatography were pooled and concentrated under reduced pressure, $T < 313$ K. Ion exchange chromatography was performed on Dowex1X2100-OH⁻ resin (Sigma Aldrich). The resin was purchased as the Cl⁻ form and converted to the OH⁻ form by treatment with aqueous NaOH. ¹H and ¹³C NMR spectra (assigned by 2D DQF-COSY and HMQC techniques) were run on a Varian Unity Plus 300 NMR spectrometer, operating at 299.938 MHz and 75.428 MHz, for ¹H and ¹³C, respectively. Chemical shifts (δ) are given in ppm relative to the CDCl₃ solvent (¹H, δ 7.27; ¹³C, δ 77.36) as internal

standard. For ^1H and ^{13}C spectra recorded in D_2O , chemical shifts (δ) are given in ppm relative to TSP as internal reference (^1H , $\delta 0.0$) and *tert*-butanol as external reference (^{13}C , $\text{CH}_3\delta 30.29$).

Synthesis of methyl 3-hydroxy-2-(4-(pyren-1-yl)butanamido)propanoate (3):

To a solution of HCl,H-Ser-OMe (**1**) (5.0 mmol, 0.778 g) and triethylamine (10 mmol) in acetonitrile (5.0 mL), was added 1-pyrenebutyric acid (**2**) (5.0 mmol, 1.44 g), 1-hydroxybenzotriazole (HOBt) (5.0 mmol, 0.675 g) and dicyclohexylcarbodiimide (DCC) (5.5 mmol, 1.13 g). The reaction mixture was left stirring at room temperature for 18 hours. The reaction mixture was filtered and the solvent was removed under reduced pressure. The residue was dissolved in ethyl acetate (100 mL), washed with KHSO_4 1M, NaHCO_3 1M and brine (3 x 30 mL each) and dried over MgSO_4 . The solvent was removed to give **3** (1.70 g, 87%) as a yellow oil. ^1H NMR (300 MHz, CDCl_3): $\delta = 2.17\text{-}2.26$ (m, 2H, CH_2), 2.37 (t, $J=7.2$ Hz, 2H, CH_2), 3.35-3.41 (m, 2H, CH_2), 3.76 (s, 3 H, CH_3), 3.86-4.00 (m, 2 H, $\beta\text{-CH}_2$ Ser), 4.66-4.71 (m, 1 H, $\alpha\text{-CH}$ Ser), 6.49 (d, $J=7.2$ Hz, 1H, NH), 7.84 (d, $J=7.8$ Hz, 1H, ArH), 7.96-8.02 (m, 3H, ArH), 8.08-8.17 (m, 4H, ArH), 8.28 (d, $J=9.3$ Hz, 1H, ArH) ppm. ^{13}C NMR (75.4 MHz, CDCl_3): $\delta = 27.14$ (CH_2), 32.58 (CH_2), 35.69 (CH_2), 52.72 (CH_3), 54.61 (CH), 63.40 (CH_2), 123.28 (CH), 124.74 (CH), 124.75 (CH), 124.88 (CH), 124.91 (C), 125.02 (C), 125.81 (CH), 126.68 (CH), 127.33 (CH), 127.37 (CH), 127.42 (CH), 128.70 (C), 129.91 (C), 130.82 (C), 131.24 (C), 135.61 (C), 170.93 (C=O), 173.20 (C=O) ppm. HRMS (ESI): m/z : calcd. for $\text{C}_{24}\text{H}_{23}\text{NNaO}_4$, $[\text{M}+\text{Na}]^+$: 412.1520; found 412.1519.

Synthesis of methyl 2-[*N*-(*tert*-butoxycarbonyl)-4-(pyren-1-yl)butanamido]acrylate (4):

To a solution of Pyr-Ser-OMe (**3**) (5.0 mmol, 1.95 g) in dry acetonitrile (5.0 mL) was added 4-dimethylaminopyridine (DMAP) (1.7 mmol, 0.213 g) and *tert*-butyldicarbonate (17.5 mmol, 3.82 g). The reaction mixture was left stirring at room temperature for 24 hours. The solvent was removed under reduced pressure and the residue was dissolved in ethyl acetate (100 mL). The organic layer was washed with KHSO_4 1M, NaHCO_3 1M and brine (3 x 30 mL, each), dried over MgSO_4 and the solvent removed under reduced pressure to give **4** (1.91 g, 81%) as a yellow oil. ^1H NMR (400 MHz, CDCl_3): $\delta = 1.46$ (s, 9 H, CH_3 Boc), 2.23-2.27 (m, 2H, CH_2), 3.17 (t, $J= 6.8$ Hz, 2H, CH_2), 3.42-3.46 (m, 2H, CH_2), 3.81 (s, 3H, OCH_3), 5.67 (s, 1H, CH_2), 6.48 (s, 1H, CH_2), 7.91 (d, $J= 7.6$ Hz, 1H, ArH), 7.98-8.06 (m, 3H, ArH), 8.11-8.13 (m, 2H, ArH), 8.16-8.18 (m, 2H, ArH), 8.37 (d, $J= 9.2$ Hz, 1H, ArH) ppm. ^{13}C NMR (100.6 MHz, CDCl_3): $\delta = 26.82$ (CH_2), 27.81 [$\text{C}(\text{CH}_3)_3$], 32.91 (CH_2), 37.44 (CH_2), 52.47 (OCH_3), 83.72 [$\text{OC}(\text{CH}_3)_3$], 123.56 (CH), 124.67 (CH), 124.77 (CH), 124.79 (CH_2), 124.99 (C),

125.06 (C), 125.74 (CH), 125.90 (CH), 126.58 (CH), 127.29 (CH), 127.34 (CH), 127.47 (CH), 128.77 (C), 129.88 (C), 130.93 (C), 131.40 (C), 135.55 (C), 136.29 (C), 151.52 (C=O), 163.68 (C=O), 175.21 (C=O) ppm. HRMS (ESI): m/z : calcd. for $C_{29}H_{29}NNaO_5$, $[M+Na]^+$: 494.1943; found 494.1929.

Synthesis of (2-(*N*-*t*-butoxycarbonyl)pyrenebutyramido)-methoxycarbonylethyl-1,4,7,10-tetrazacyclododecane (monoalkylated cyclen) (6): K_2CO_3 (1.47 g, 10.6 mmol) was added to a solution of cyclen (5) (0.460 g, 2.67 mmol) in MeCN (30 mL). To this solution was added (pyrene)Boc- Δ -AlaOMe (4) (0.840 g, 1.78 mmol). The suspension was vigorously stirred at room temperature for 5 hours. The suspended solid was removed by filtration and the solvent was evaporated under reduced pressure. The residue was purified by flash chromatography (100% $CH_2Cl_2 \rightarrow CH_2Cl_2/EtOH/NH_4OH/H_2O$ (50:50:1:1)) to afford compound 6 as a viscous light yellow oil (0.95 g, 83%). 1H NMR (300 MHz, $CDCl_3$): δ = 1.47 (s, 9H, Boc), 2.20 (m, 2H, $CH_2CH_2CH_2$), 2.50-2.80 (m, 16H, $N(CH_2)_2N$ -cyclen), 3.01-3.18 (m, 2H, $C(O)CH_2CH_2$), 3.38-3.50 (m, 2H, CH_2CH_2 -Pyrene), 2.77 (dd, J = 14.4 and 6.9 Hz, 1 H, NCH_aH_bCH), 3.38 (dd, J = 14.25 and 5.1 Hz, 1 H, NCH_aH_bCH), 3.70 (s, 3H, OMe), 5.51 (t, J = 6.9 and 4.8 Hz, 1H, NCH_aH_bCH), 7.85-8.40 (9H, m, Ar). ^{13}C NMR (75.4 MHz, $CDCl_3$): δ = 26.98 (βCH_2 -Ser), 27.88 ($C(CH_3)_3$), 32,85 (γCH_2), 37,79 (αCH_2), 45.02 (CH_2), 45.37 (CH_2), 46.75 (CH_2), 51.22 (CH_2), 52.22 (OCH₃), 53.52 (CH), 55.97 (NCH_2CH), 84.31 ($C(CH_3)_3$), 123,41 (CH-Ar), 124,70 (CH-Ar), 124.72 (CH-Ar), 124,87 (CH-Ar), 125,83 (CH-Ar), 126,67 (CH-Ar), 127.37 (2x(CH-Ar)), 127,45 (CH-Ar), 128,01 (C-Ar), 128,62 (C-Ar), 129.86 (C-Ar), 130,82 (C-Ar), 131.31 (C-Ar), 136.13 (C-Ar), 151.86 (NC(O)), 170.63 ($C(O)OCH_3$), 175,37 ($C(O)CH_2$). HRMS (ESI): m/z : calcd for $C_{37}H_{50}N_5O_5$, $[M+H]^+$: 644.3812, found: 644.3807.

Synthesis of 2-pyrenebutyramido-methoxycarbonylethyl-4,7,10-tris-(ethoxycarbonylmethyl)-1,4,7,10 tetrazacyclododecane (tetraalkylated cyclen) (7):

A solution of monoalkylated cyclen (6) (0.860 g, 1.33 mmol) in trifluoroacetic acid in dichlorometane (60%, 25 mL) was stirred overnight at room temperature. The solvent was evaporated at reduced pressure and the residue was re-dissolved in dichlorometane. This procedure was repeated several times to give a light yellow thick oil. 1H NMR spectroscopy ($CDCl_3$) revealed the disappearance of the signal assigned to the *tert*-butoxycarbonyl group in compound 6. K_2CO_3 (2.20 g, 15.96 mmol) was added to a solution of deprotected 6 (1.33 mmol, quantitative deprotection was assumed) in MeCN (30 mL). To this suspension was added ethyl bromoacetate (0.55 mL, 4.66 mmol). The suspension was vigorously stirred at room temperature for 2.5 hours. The solid in suspension was removed by filtration, the solvent was evaporated under reduced pressure and the residue was purified by flash

chromatography (100% CH₂Cl₂ → CH₂Cl₂/EtOH (1:1)) to afford compound **7** (0.632 g, 59%) as a white foam. ¹H NMR (300 MHz, CDCl₃): δ = 1.26 (m, 9H, 3xCH₂CH₃), 2.20 (m, 2H, CH₂CH₂CH₂), 2.56 (m, 2H, C(O)CH₂CH₂), 2.60-2.90 (m, 6H, NCH₂C(O)), 2.90-3.70 (m, 16H, N(CH₂)₂N), 3.37 (m, 2H, CH₂CH₂Pyrene), 3.73 (s, 3H, OMe), 3.92 (bd, 2H, NCH₂CH), 4.09 (m, 6 H, CH₂CH₃), 4.94 (bd, 1H, NCH₂CH), 7.80-8.40 (9H, m, Ar). ¹³C NMR (75.4 MHz, CDCl₃): selected signals: 13.84, 13.88, 14.05 (CH₂CH₃), 27.36 (βCH₂-Ser), 32,79 (γCH₂), 35,45 (αCH₂), 48.21 (CH), 48.91 (CH₂), 50.34 (CH₂), 51.36 (CH₂), 52.47 (OCH₃), 53.01 (CH₂), 53.60 (CH₂CH), 54.90 (CH₂), 55.19 (CH₂), 55.71 (CH₂), 55.98 (CH₂), 58.25 (CH₂), 60.51 (CH₂), 60.99, 61.20, 61.55 (OCH₂), 123,63 (CH-Ar), 124,62 (CH-Ar), 124.75 (CH-Ar), 124,85 (CH-Ar), 125,76 (CH-Ar), 126,51 (CH-Ar), 127.18 (CH-Ar), 127,41 (CH-Ar), 127,46 (CH-Ar), 128,67 (C-Ar), 129,72 (C-Ar), 130.87 (C-Ar), 131.32 (2x(C-Ar)), 136.43 (C-Ar), 136.53 (C-Ar), 170.312 (C(O)OCH₃), 170.53 (C(O)OCH₂), 173.15 (C(O)OCH₂), 173.55 (C(O)OCH₂), 174.31 (NC(O)). HRMS (ESI): *m/z*: calcd for C₄₄H₆₀N₅O₉, [M+H]⁺: 802.4391, found: 802.4386.

Synthesis of 2-pyrenebutyramido-carboxyethyl-4,7,10-tris-(carboxymethyl)-1,4,7,10-tetrazacyclododecane (L) (DO3A-N-(α-pyrenebutyramido)propionate metal chelator):

Compound (**7**) (0.566 g, 0.710 mmol) was dissolved in a mixture made up of 20 mL of water and 20 mL of ethanol. The solution was adjusted to pH 10-11 by adding small portions of Dowex 1X2-100-OH⁻ resin. The suspension was kept stirring at room temperature for 2 hours. The wet resin was transferred into a chromatography column, washed with water (~ 50 mL) and eluted with 0.1 M hydrochloric acid, followed by a mixture of hydrochloric acid 0.1M/Etanol (1:1). The relevant fractions, identified by TLC (ethanol/water 1/1, revelation with iodine vapour and analysis under UV light 365 nm) were pooled, concentrated at room temperature and further dried under vacuum to afford the final compound, as hydrochloride, as a light yellow solid (0.31 g, 62%). ¹H NMR (300 MHz, D₂O/MeOD): δ= 2.13 (bb, 2H, CH₂CH₂CH₂), 2.50 (m, 2H, C(O)CH₂CH₂), (2.9-3.6, broad, overlapped signals with a integration corresponding to, 18H, 4xN(CH₂)₂N and NCH₂CH), 3.33 (m, 2H, CH₂CH₂Pyrene), 3.81 (broad, overlapped signals with a integration corresponding to 6H, NCH₂), 4.76 (m (br), 1H, CH), 7.80-8.40 (9H, m, Ar). ¹³C NMR (75.4 MHz, D₂O/MeOD): selected signals: 28.22 (βCH₂), 33,25 (γCH₂), 36,29 (αCH₂), 50.49 (bb, CH₂), 54.95 (bb, CH₂), 124,31 (CH-Ar), 125,44 (C-Ar), 125,54 (C-Ar), 125,75 (CH-Ar), 125.85 (2x(CH-Ar)), 127,08 (CH-Ar), 127,50 (CH-Ar), 127.08 (C-Ar), 128,18 (CH-Ar), 128.37 (CH-Ar), 128,46 (CH-Ar), 129.41 (C-Ar), 130.75 (C-Ar), 131.75 (C-

Ar), 137.27 (C-Ar), 177.47 (NC(O)). HRMS (ESI): m/z : calcd for $C_{37}H_{46}N_5O_9$, $[M + H]^+$: 704.3296, found: 704.3290.

1H and ^{17}O NMR and 1H NMRD experiments

Sample preparation

To an aqueous solution of the ligand (pH 5) was added drop-wise an aqueous solution of the corresponding $LnCl_{3.x}H_2O$ salt in a 1:1 mole ratio. The solution was stirred at room temperature over 1 hour while keeping its pH at around 5.7 by adding aqueous NaOH. The solution was left stirring at room temperature overnight. Concentration under reduced pressure afforded off-white solids. Solutions for NMR measurements (20 mM) were obtained by dissolution of appropriate amounts of solid complexes in D_2O ($V = 0.75$ mL). Proton 1D spectra of paramagnetic (Sm^{3+} and Eu^{3+}) and diamagnetic (La^{3+}) complexes were obtained at 298 K on a Varian VNMRs 600 (14.09 T, 600.14 MHz) NMR spectrometer.

The GdL complex solutions for ^{17}O NMR and 1H NMRD experiments were prepared by mixing equimolar amounts of $GdCl_3$ and ligand. A slight excess (5%) of ligand was used. The solution was stirred at room temperature over 1 hour while keeping its pH at around 5.7 by adding aqueous NaOH. The solution was left stirring at room temperature overnight. The absence of free metal was checked by the xylenol orange test.^{56,57} The pH of the stock solution was adjusted to the desired value by adding aqueous NaOH (0.1 mM). ^{17}O -enriched water (^{17}O : 11.4%) was added to the solutions for ^{17}O measurements to improve sensitivity. The final concentration of the complex solution was 17.56 mmol kg^{-1} at pH = 6.90. For the NMRD experiments 5.0 mM and 0.1 mM solutions of the complex at pH 6.98 were used.

^{17}O NMR experiments

Variable-temperature ^{17}O NMR measurements were performed on a Bruker Avance-500 (11.7 T) spectrometer. A BVT-3000 temperature control unit was used to stabilize the temperature, measured by a substitution technique. The samples were sealed in glass spheres that fitted into 10 mm o.d. NMR tubes to eliminate susceptibility corrections to the chemical shifts.⁵³ Longitudinal relaxation rates ($1/T_1$) were obtained by the inversion recovery method, and transverse relaxation rates ($1/T_2$) by the Carr-Purcell-Meiboom-Gill spin-echo technique. Acidified water, pH 3.4, was used as external reference.

NMRD measurements

The measurements were performed using a Stellar Spinmaster FFC NMR relaxometer (0.01–20 MHz) equipped with a VTC90 temperature control unit. At higher fields, the ^1H relaxivity measurements were performed on a Bruker Electromagnet at the frequencies of 30 MHz, 40 MHz, 60 MHz and 80 MHz. In each case, the temperature was measured by a substitution technique. Variable temperature measurements were performed at 25 and 37°C.

Relaxivity studies of pH dependence and Zn^{2+} transmetallation

The transmetallation reaction of GdL with Zn^{2+} was studied by following the time dependent decrease of the water proton longitudinal relaxation rate, R_1 , of a phosphate-buffered saline solution (PBS, pH 7.1, 10 mM) containing 1.5 mM of GdL after adding an equimolar amount of ZnCl_2 while the sample was vigorously stirred.⁵⁹ The water longitudinal relaxation rate was also measured as a function of time on the PBS buffered solution (pH 7.1, 10 mM) containing 2.5 mM GdL.⁶⁰ The pH dependence of the relaxivity of the GdL solution was studied by adjusting (pH meter) the pH of a 1 mM solution of GdL in water with either NaOH or HCl solutions using a pH meter. A Bruker Minispec mq20 (20 MHz, 298 K) relaxometer was used for all measurements.

Fluorescence Measurements

The absorption and the ligand-based fluorescence emission spectra of the free ligand L and the GdL complex were recorded, respectively, with a Jasco V-630 UV-Vis spectrophotometer and a HORIBA JobinYvon Fluoromax-4 spectrofluorimeter, equipped with a monochromator in both excitation and emission and a temperature controlled cuvette holder. Fluorescence spectra were corrected for the instrumental response of the system.

The fluorescence quantum yields (Φ_s) were determined using the standard method.^{61,62} Anthracene in ethanol ($\Phi_r = 0.27$)⁶³ was used as reference.

For the lanthanide centred fluorescence studies in the visible (Eu^{3+} and Tb^{3+}) and in the NIR region (Nd^{3+} , Yb^{3+}), absorbance UV spectra were performed on an Uvikon spectrophotometer, while emission and excitation (lanthanide luminescence) spectra were measured using a modified Jobin-Yvon Horiba Fluorolog-322 spectrofluorimeter equipped with a Hamamatsu R928 detector (for the visible domain) and a DSS-IGA020L (Electro-Optical Systems, Inc.) detector (for the NIR domain). Luminescence and excitation spectra were corrected for variations in lamp output, non-linear response of the detector and the use of neutral density filters (where applicable). For collecting luminescence data, samples were placed into quartz Suprasil cells (Hellma[®] 115F-QS, bandpass 0.2 cm).

Biodistribution studies

^{153}SmL for *in vivo* experiments was prepared by adding 1 mCi of [^{153}Sm]Cl₃ (produced at the Instituto Tecnológico e Nuclear, Lisbon, Portugal with a specific radioactivity > 5 GBq/mg) to a solution of 1 mg of the chelator in acetate buffer (400 μL , 0.4 M, pH 5) and heated at 80 °C for ca 1 hour. The radiochemical purity of $^{153}\text{SmL}_1$ was determined by TLC. The percentage of chelated metal was found to be greater than 95%.

Groups of four animals (Wistar rat males weighting ca 200 g) were anaesthetized with Ketamine (50.0 mg/mL)/chlorpromazine (2.5%) (10:3) and injected in the tail vein with ca 100 μCi of the tracer. Animals were sacrificed 1 and 24 hours later and the major organs were removed, weighted and counted in a γ well-counter.

Size distribution

The size distribution of particles in a (micellar) solution of GdL at a concentration well above the *cmc* (5.0 mM, pH 7.0) was determined with a Malvern Zetasizer, NANO ZS (Malvern Instruments Limited, UK), using a He-Ne laser ($\lambda = 633$ nm) and a detector angle of 173°. The GdL solution in a polystyrene cell (1 mL) was analysed at 25 °C. The mean hydrodynamic radius (z-average) and a width parameter for the distribution, polydispersity or polydispersity Index (PDI) were calculated from the intensity of the scattered light. In the present work, the intensity-based z-average parameter was considered the best approach to the actual particle size.

Data Analysis. Data obtained in ^{17}O NMR, ^1H NMRD, Luminescence and Quantum Yield measurement studies were processed in OriginLab Pro 8 SRO. Data from relaxometric and transmetallation studies were processed with Microsoft Office Excel 2007.

Acknowledgements

This work was financially supported by Fundação para a Ciência e Tecnologia, Portugal: PEst-C/QUI/UI0686/2013; FCOMP-01-0124-FEDER-037302; PTDC/QUI/70063/2006; grant SFRH/BD/63994/2009 to Miguel Ferreira and sabbatical grant SFRH/BSAB/1328/2013 to J. A. Martins; Rede Nacional de RMN (REDE/1517/RMN/2005) for the acquisition of the Varian VNMRs 600 NMR spectrometer at the University of Coimbra and the Bruker Avance-3 400 Plus at the University of Minho in Braga. The work in France was supported by La Ligue contre le Cancer. S. Petoud acknowledges support from the Institut National de la Santé ET de la Recherche Médicale (INSERM). This work was carried out in the framework of the COST Actions D38 “Metal Based Systems for Molecular Imaging”, TD1004 “Theranostic Imaging” and CM1006 “EUFEN: European F-Element Network”.

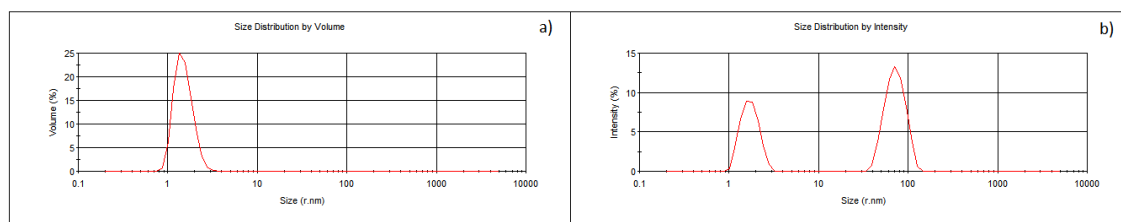
References

- 1- M. L. James, S. S. Gambhir, *Physiol. Rev.* 2012, **92**, 897.
- 2- P. Caravan, J. J. Ellison, T. J. McMurry, R. B. Lauffer, *Chem. Rev.*, 1999, **99**, 2293.
- 3- The Chemistry of Contrast Agents in Medical Magnetic Resonance Imaging, A. Merbach, L. Helm, É. Tóth, Eds., 2nd edition, Chichester: Wiley; 2013.
- 4- L. Helm, *Progr. Nucl. Magn. Reson. Spectrosc.*, 2006, **49**, 45.
- 5- P. Marckmann, L. Skov, K. Rossen, A. Dupont, M. B. Damholt, J. G. Heaf, H. S. Thomsen, *J. Am. Soc. Nephrol.* 2006, **17**, 2359.
- 6- J. C. Weinreb, A. K. Abu-Alfa, *J. Magn. Reson. Imaging*, 2009, **30**, 1236.
- 7- M. Port, J.-M. Idée, C. Medina, C. Robic, M. Sabatou, C. Corot, *BioMetals*, 2008, **21**, 469.
- 8- S. K. Morcos, *Eur. J. Radiology*, 2008, **66**, 175.
- 9- P. Caravan, C. T. Farrar, L. Frullano, R. Uppal, *Contrast Media & Mol Imag* 2009, **4**, 89.
- 10- A. Borel, J. F. Bean, R. B. Clarkson, L. Helm, L. Moriggi, A. D. Sherry, M. Woods, *Chem. Eur. J.* 2008, **14**, 2658.
- 11- S. Torres, J. A. Martins, J. P. André, C. F. G. C. Geraldes, A. E. Merbach, E. Tóth, *Chem. Eur. J.* **2006**, **12**, 940.
- 12- E. Boros, P. Caravan, *J. Med. Chem.*, 2013, **56**, 1782.
- 13- Z. Zhang, M. T. Greenfield, M. Spiller, T. J. McMurry, R. B. Lauffer, P. Caravan, *Angew. Chem. Int. Ed.*, 2005, **44**, 6766.
- 14- É. Tóth, D. Pubanz, S. Vauthey, L. Helm, A. E. Merbach, *Chem. Eur. J.*, 1996, **2**, 1607.
- 15- M. F. Ferreira, B. Mousavi, P. M. Ferreira, C. I. O. Martins, L. Helm, J. A. Martins, C. F. G. C. Geraldes, *Dalton Trans.*, 2012, **41**, 5472.
- 16- S. Qazi, L. O. Liepold, M. J. Abedin, B. Johnson, P. Prevelige, J. A. Frank, T. Douglas, *Mol. Pharmaceutics*, 2013, **10**, 11.
- 17- G. J. Stasiuk, S. Tamang, D. Imbert, C. Poillot, M. Giardiello, C. Tisseyre, E. L. Barbier, P. H. Fries, M. de Waard, P. Reiss, M. Mazzanti, *ACS Nano*, 2011, **5**, 8193.
- 18- M. F. Ferreira, A. F. Martins, J. A. Martins, P. M. Ferreira, E. Toth, C. F. G. C. Geraldes, *Chem. Commun.* 2009, 6475.
- 19- Z. Jaszberenyi, A. Sour, É. Tóth, M. Benmelouka, A. E. Merbach, *Dalton Trans.* 2005, **16**, 2713.
- 20- E. Balogh, R. Tripier, P. Fouskova, F. Reviriego, H. Handel, É. Tóth *Dalton Trans.* 2007, 3572.
- 21- M.F. Ferreira, A.F. Martins, C.I.O. Martins, P.M. Ferreira, É. Tóth, T.B. Rodrigues, D. Calle, S. Cerdan, P. Lopez-Larrubia, J.A. Martins, C.F.G.C. Geraldes, *Contrast Med. Mol. Imaging*, 2013, **8**, 40.
- 22- A. Louie, *Chem. Rev.*, 2010, **110**, 3146.
- 23- Y. Song, H. Zong, E. R. Trivedi, B. J. Vesper, E. A. Waters, A. G. M. Barrett, J. A. Radosevich, B. M. Hoffman, T. J. Meade, *Bioconjugate Chem.* 2010, **21**, 2267.

-
- 24- W. J. M. Mulder, R. Koole, R. J. Brandwijk, G. Storm, P. T. K. Chin, G. J. Strijkers, C. M. Donega, K. Nicolay, A. W. Griffioen, *Nano Lett.* 2006, **6**, 2.
- 25- S. L. C. Pinho, H. Faneca, C. F. G. C. Geraldés, M. -H. Delville, L. D. Carlos, J. Rocha, *Biomaterials*, 2012, 33, 925.
- 26- E. Lipani, S. Laurent, M. Surin, L. Vander Elst, P. Leclère, R. N. Muller, *Langmuir*, 2013, **29**, 3419.
- 27- F. M. Winnik, *Chem. Rev.* 1993, **93**, 587.
- 28- J. Duhamel, *Langmuir*, 2012, **28**, 6527.
- 29- Z. Wang, P. Huang, A. Bhirde, A. Jin, Y. Ma, G. Niu, N. Neamati, X. Chen *Chem. Commun.*, 2012, **48**, 9768.
- 30- S. Karuppannan, J.-C. Chambron, *Chem. Asian J.* 2011, **6**, 964.
- 31- S. Faulkner, M.-C. Carrié, S. J. A. Pope, J. Squire, A. Beeby, P. G. Sammes, *Dalton Trans.*, 2004, 1405.
- 32- S. J. A. Pope, *Polyhedron*, 2007, **26**, 4818.
- 33- P. M. T. Ferreira, H. L. S. Maia, *J. Chem. Soc.-Perkin Trans.*, 1999, **1**, 3697.
- 34- E. Boros, M. Polasek, Z. Zhang, P. Caravan, *J. Am. Chem. Soc.*, 2012, **134**, 19858.
- 35- F. A. Dunand, E. Tóth, R. Hollister, A. E. Merbach, *J. Biol. Inorg. Chem.*, 2001, **6**, 247.
- 36- D. H. Powell, O. M. N. Dhubhghaill, D. Pubanz, L. Helm, Y. S. Lebedev, W. Schlaepfer, A. E. Merbach, *J. Am. Chem. Soc.*, 1996, **118**, 9333.
- 37- J. P. André, E. Tóth, H. Fischer, A. Seelig, H. R. Mäcke, A. E. Merbach, *Chem. Eur. J.*, 1999, **5**, 2977.
- 38- L. Tei, G. Gugliotta, Z. Baranyai, M. Botta, *Dalton Trans.*, 2009, **44**, 9712.
- 39- C. Vanasschen, N. Bouslimani, D. Thonon, J. F. Desreux, *Inorg. Chem.*, 2011, **50**, 8946.
- 40- F. Kielar, L. Tei, E. Terreno, M. Botta, *J. Am. Chem. Soc.*, 2010, **132**, 7836.
- 41- J. P. Holland, V. Fisher, J. A. Hickin, J. M. Peach, *Eur. J. Inorg. Chem.* 2010, 48.
- 42- C. Wang, S. D. Wettig, M. Foldvari, R. E. Verrall, *Langmuir*, 2007, **23**, 8995.
- 43- P. Carpena, J. Aguiar, P. Bernaola-Galván, C. Carnero Ruiz, *Langmuir*, 2002, **18**, 6054.
- 44- C. Keyes-Baig, J. Duhamel, S. Wettig, *Langmuir*, 2011, **27**, 3361.
- 45- K. Lim, A. Price, S.-F. Chong, B. M. Paterson, A. Caragounis, K. J. Barnham, P. J. Crouch, J. M. Peach, J. R. Dilworth, A. R. White, P. S. Donnelly, *J. Biol. Inorg. Chem.*, 2010, **15**, 225.
- 46- J.-C. G. Bunzli, *Chem. Rev.*, 2010, **110**, 2729.
- 47- R. B. Lauffer, D. J. Parmelee, S. U. Dunham, H. S. Quellet, R. P. Dolan, S. White, T. J. McMurry, R. C. Walovitch, *Radiology*, 1988, **207**, 529.
- 48- V. Henrotte, L. Vander Elst, S. Laurent, R. N. Muller, *J. Biol. Inorg. Chem.*, 2007, **12**, 929.
- 49- P. Caravan, N.J. Cloutier, M.T. Greenfield, S.A. McDermid, S.U. Dunham, J.W.M. Bulte, J.C. Amedio Jr, R.J. Looby, R.M. Supkowski, R.M. Horrocks RM Jr, T.J. McMurry, R.B. Lauffer, *J. Am. Chem. Soc.*, 2002, **124**, 3152.
- 50- L. Moriggi, M.A. Yaseen, L. Helm, P. Caravan, *Chem. Weinh. Bergstr. Ger.* 2012, **18**, 3675.
- 51- M. Giardiello, M. Botta, M.P. Lowe, *J. Incl. Phenom. Macrocycl. Chem.* 2011, **71**, 435.

-
- 52-** A.F. Martins, J.-F. Morfin, A. Kubíčková, V. Kubíček, F. Buron, F. Suzenet, M. Salerno, A.N. Lazar, C. Duyckaerts, N. Arlicot, D. Guilloteau, C.F.G.C. Geraldès, É. Tóth, *ACS Med. Chem. Lett.*, 2013, 5, 436.
- 53-** R. Wegrzyn, A. Nyborg, D. R. Duan, A. Rudolf, US Patent US8062895
- 54-** S. Torres, M. I. M. Prata, A. C. Santos, J. P. André, J. A. Martins, L. Helm, E. Tóth, M. L. García-Martín, T. B. Rodrigues, P. López-Larrubia, S. Cerdán, C. F. G. C. Geraldès, *NMR in Biomed.* 2008, **21**, 322.
- 55-** Furukawa, Y. Ueno, E. Tamechika, H. Hibino, *J. Mater. Chem. B*, 2013, **1**, 1119.
- 56-** R. Hovland, A. J. Aasen, J. Klaveness, *Org & Biomol Chem.* 2003, **1**, 1707.
- 57-** A. Barge, G. Cravotto, E. Gianolio, F. Fedeli, *Contrast Media & Mol Imag.* 2006, **1**, 184.
- 58-** A. D. Hugi, L. Helm, A. E. Merbach, *Inorg. Chem.*, 1987, **26**, 1763.
- 59-** S. Laurent, L. V. Elst, F. Copoix, R. N. Muller, *Invest Radiol.* 2001, **36**, 115.
- 60-** S. Laurent, L. V. Elst, A. Vroman, R. N. Muller, *Helv. Chim. Acta* 2007, 90, 562.
- 61-** J. N. Demas, G. A. Crosby, *J. Phys. Chem.* 1971, **75**, 991.
- 62-** S. Fery-Forgues, D. Lavabre, *J. Chem. Educ.* 1999, **76**, 1260.
- 63-** J. V. Morris, M. A. Mahaney, J. R. Huber, *J. Phys. Chem.* 1976, **80**, 969.

Supplementary Information



	z-average (r. nm)	Radius (nm) (% volume)	Radius (nm) (% intensity)
GdL (5 mM, pH 7.0, 25 °C)	48.9	1.57 (100%)	73.1 (61.9%) 1.74 (38.1%)

Figure S1. Size distribution in: a) volume (%); b) intensity (%) for a GdL solution (5.0 mM, pH 7.0, 25 °C) at a concentration well above the *cmc* (0.6 mM).

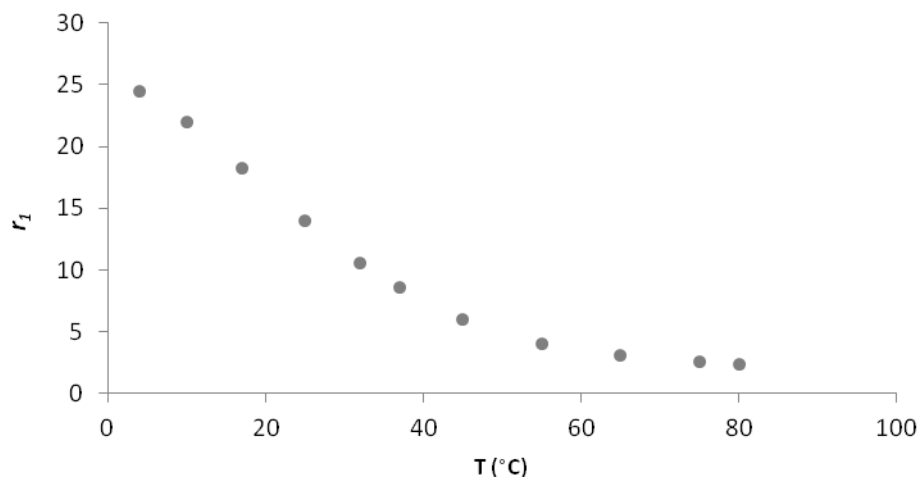


Figure S2. Temperature dependence of the water proton relaxivity for GdL (20MHz , 1mM, pH 6.0).

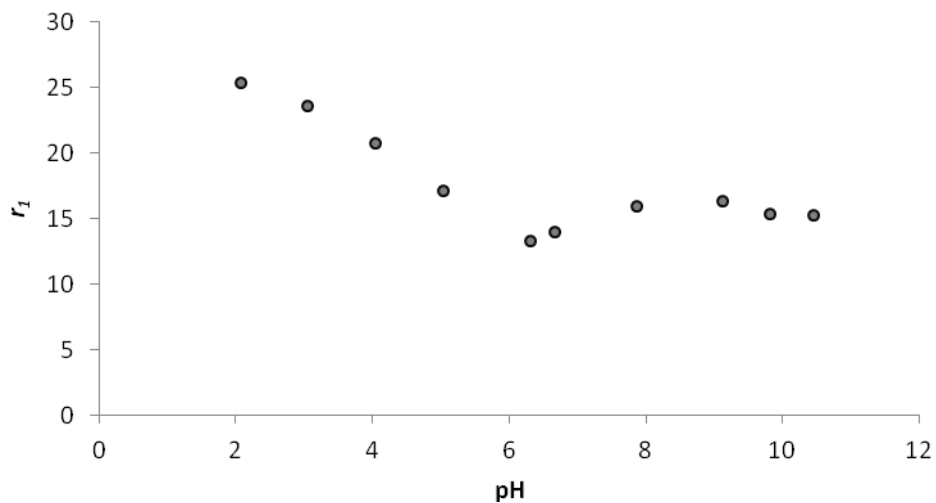


Figure S3. pH dependence of the water proton relaxivity for GdL (20 MHz, 1 mM, 25 °C).

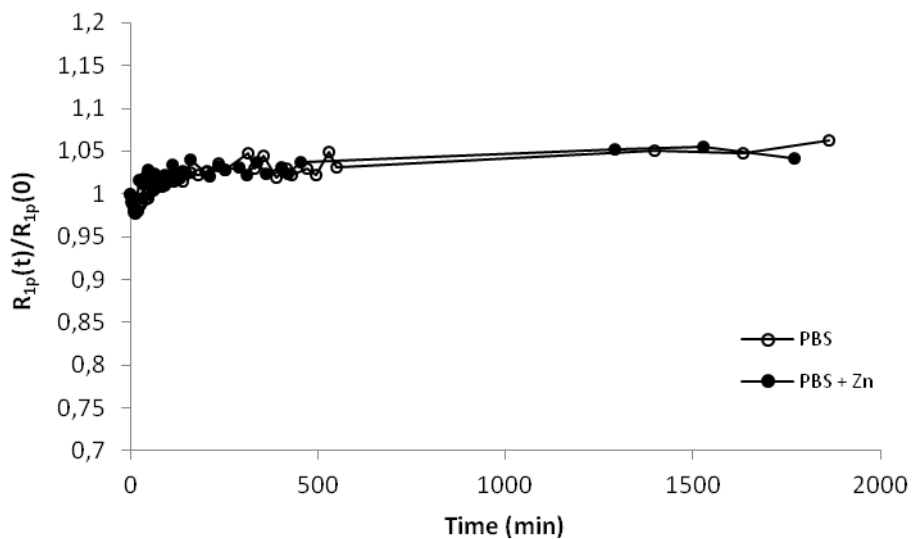


Figure S4. Evolution of the relative water proton paramagnetic longitudinal relaxation rate $R_{1p}(t)/R_{1p}(0)$ (20 MHz, pH 7.1, 25 °C) for a 1.5 mM solution of GdL in 10 mM phosphate buffer(○) and in phosphate buffer containing an equimolar amount of Zn^{2+} (●).

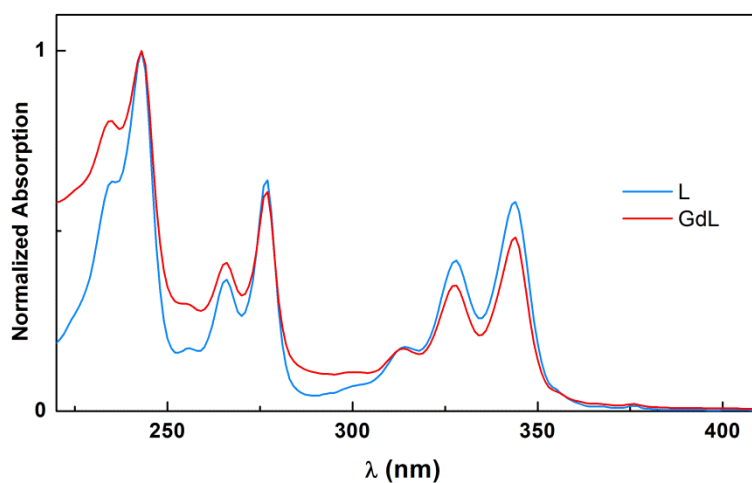


Figure S5. UV-Vis spectra for the free ligand **L** and for the Gd**L** complex in water (1.0×10^{-5} M, pH 7.0, 25 °C).

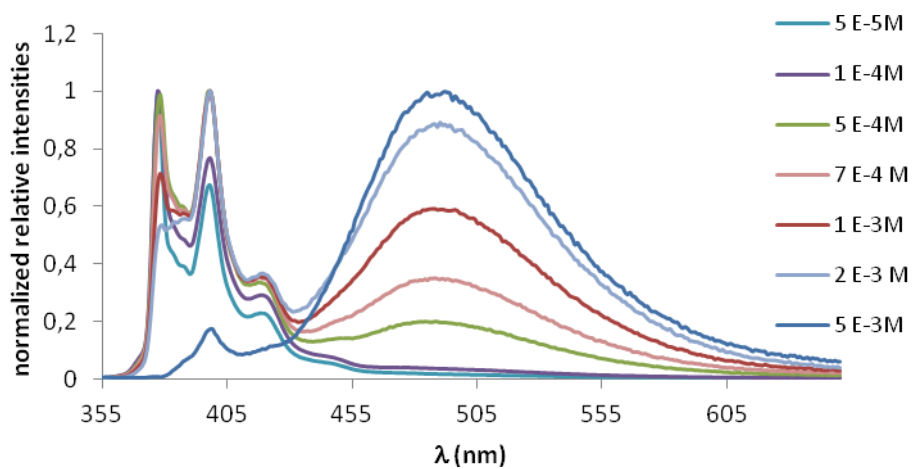


Figure S6. Fluorescence spectra for free ligand **L** in non-deoxygenated water (pH 7.0, 25 °C) over the concentration range 5×10^{-5} - 5×10^{-3} mol.dm⁻³ ($\lambda_{exc} = 345$ nm).

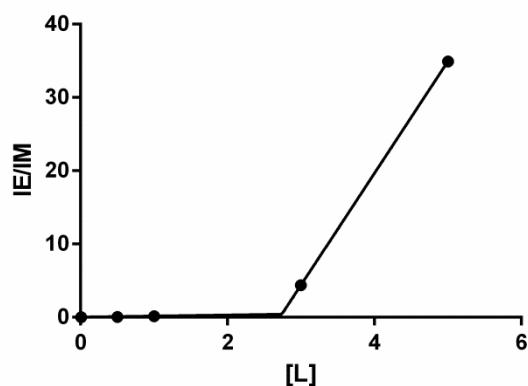


Figure S7. Changes in the emission properties of the free ligand **L** as the ratio of the fluorescence emission intensity for the excimer (490 nm) and for the monomer (377 nm) (I_E/I_M) as function of ligand concentration. Line fitted to **equation S1**.

The experimental data in **Figure 5** (manuscript) and **Figure S6** were fitted (Prima GraphPad) to a sigmoidal model (**equation S1**).^[1,2]

$$\left(\frac{I_{Exc}}{I_{Mono}} \right) = \left(\frac{I_{Exc}}{I_{Mono}} \right)_0 + A_1 c + d(A_2 - A_1) \ln \left(\frac{1 + e^{\frac{(c-cmc)/d}}}{e^{-cmc/d}} \right)$$

Equation S1

c - complex (GdL) or free ligand (**L**) concentration;

A_1 and A_2 - represent the limits of sigmoidal function that describes the behaviour of $d(I_{Exc}/I_{Mono})/dc$ (derivative of I_{Exc}/I_{Mono} in order to c);

d - is the time constant of the function and is related to the range of concentration over which the abrupt change in I_{Exc}/I_{Mono} occurs;

cmc - is the center of the sigmoidal function.

Table S1. Best fit values for the fitting (Prima GraphPad) of the experimental data of I_{Exc}/I_{Mono} vs [GdL] (**Figure 5** in manuscript and **Figure S6**) to **equation S1**.

Best-fit values	GdL
$(I_{Exc}/I_{Mono})_0$	-1.764
A_1	0.3660
d	0.007795
A_2	3.119
cmc	0.6454
Std. Error	
$(I_{Exc}/I_{Mono})_0$	0.007529
A_1	0.06346
d	71873
A_2	0.002088
cmc	0.01454

The E titration data (**Figure 7** in manuscript) were fitted to **equation S2** with n , number of equivalent binding sites, fixed to 1.

$$R_1^{pobs} = 10^3 \times \left\{ \left(r_1^f \cdot c_1 \right) + \frac{1}{2} \left(r_1^e - r_1^f \right) \times \left(n \cdot c_{HSA} + c_1 + K_A^{-1} - \sqrt{\left(n \cdot c_{HSA} + c_1 + K_A^{-1} \right)^2 - 4 \cdot n \cdot c_{HSA} \cdot C_1} \right) \right\}$$

Equation S2

n - number of equivalent binding sites, fixed to 1 in the fitting.
 r_1^f - relaxivity of the free GdL form, non-complexed with HSA
 r_1^e - relaxivity of the GdL form bound to HSA
 c_1 - analytical concentration of GdL
 c_{HSA} - analytical concentration of HSA
 K_A - association constant GdL/HSA

Table S2. Biodistribution, stated as percentage of injected dose per gram of organ (%ID/g \pm SD), of ^{153}SmL in Wistar rats at 1 and 24 hours after *i.v.* injection. Results are the mean of 4 animals.

Organ	1 hour %ID+SD	24 hours %ID+SD
Blood	0.3071 \pm 0.0290	0.0015 \pm 6.5x10 ⁻⁵
Liver	0.2095 \pm 0.0617	0.4701 \pm 0.1216
Spleen	0.1784 \pm 0.0581	0.3012 \pm 0.1646
Kidney	0.0629 \pm 0.0105	0.0242 \pm 0.0026
Heart	0.0385 \pm 0.0224	0.0044 \pm 0.0014
Lung	0.1084 \pm 0.0220	0.0274 \pm 0.0104
S. Intest.	0.0352 \pm 0.0190	0.0066 \pm 0.0011
L. Intest.	0.0125 \pm 0.0015	0.0035 \pm 0.0029
Bone	0.0365 \pm 0.0078	0.0411 \pm 0.0057
Muscle	0.0095 \pm 0.0048	0.011 \pm 0.00010
Brain + Cerebellum	0.0213 \pm 0.0134	0.0007 \pm 8.15x10 ⁻⁵

APPENDIX 1: Analysis of NMRD and ^{17}O NMR data

NMRD and ^{17}O NMR data have been analysed within the framework of Solomon-Bloembergen-Morgan theory.

^{17}O NMR spectroscopy

From the measured ^{17}O NMR relaxation rates and angular frequencies of the paramagnetic solutions, $1/T_1$, $1/T_2$ and ω , and of the acidified water reference, $1/T_{1A}$, $1/T_{2A}$ and ω_A , one can calculate the reduced relaxation rates and chemical shifts, $1/T_{2r}$ and $\Delta\omega_r$, which may be written as in Equations (A1)-(A3), where, $1/T_{1m}$, $1/T_{2m}$ is the relaxation rate of the bound water and $\Delta\omega_m$ is the chemical shift difference between bound and bulk water, τ_m is the mean residence time or the inverse of the water exchange rate k_{ex} and P_m is the mole fraction of the bound water. [3, 4]

$$\frac{1}{T_{1r}} = \frac{1}{P_m} \left[\frac{1}{T_1} - \frac{1}{T_{1A}} \right] = \frac{1}{T_{1m} + \tau_m} + \frac{1}{T_{1os}} \quad (\text{A1})$$

$$\frac{1}{T_{2r}} = \frac{1}{P_m} \left[\frac{1}{T_2} - \frac{1}{T_{2A}} \right] = \frac{1}{\tau_m} \frac{T_{2m}^{-2} + \tau_m^{-1} T_{2m}^{-1} + \Delta\omega_m^2}{(\tau_m^{-1} + T_{2m}^{-1})^2 + \Delta\omega_m^2} + \frac{1}{T_{2os}} \quad (\text{A2})$$

$$\Delta\omega_r = \frac{1}{P_m} (\omega - \omega_A) = \frac{\Delta\omega_m}{(1 + \tau_m T_{2m}^{-1})^2 + \tau_m^2 \Delta\omega_m^2} + \Delta\omega_{os} \quad (\text{A3})$$

The outer sphere contributions to the ^{17}O relaxation rates $1/T_{1os}$ and $1/T_{2os}$ can be neglected according to previous studies.[5] Therefore, Equations (A1-A2) can be further simplified into Equations (A4) and (A5):

$$\frac{1}{T_{1r}} = \frac{1}{T_{1m} + \tau_m} \quad (\text{A4})$$

$$\frac{1}{T_{2r}} = \frac{1}{T_{2m} + \tau_m} \quad (\text{A5})$$

The exchange rate is supposed to obey the Eyring equation. In equation (A6) ΔS^\ddagger and ΔH^\ddagger are the entropy and enthalpy of activation for the water exchange process, and k_{ex}^{298} is the exchange rate at

298.15 K.

$$\frac{1}{\tau_m} = k_{ex} = \frac{k_B T}{h} \exp\left\{\frac{\Delta S^\ddagger}{R} - \frac{\Delta H^\ddagger}{RT}\right\} = \frac{k_{ex}^{298} T}{298.15} \exp\left\{\frac{\Delta H^\ddagger}{R} \left(\frac{1}{298.15} - \frac{1}{T}\right)\right\} \quad (\text{A6})$$

In the transverse relaxation, the scalar contribution, $1/T_{2sc}$, is the most important [Equation (A7)]. $1/\tau_{s1}$ is the sum of the exchange rate constant and the electron spin relaxation rate [Equation (A8)].

$$\frac{1}{T_{2m}} \cong \frac{1}{T_{2sc}} = \frac{S(S+1)}{3} \left(\frac{A}{\hbar}\right)^2 \left(\tau_{s1} + \frac{\tau_{s2}}{1 + \omega_S^2 \tau_{s2}^2}\right) \quad (\text{A7})$$

$$\frac{1}{\tau_{s1}} = \frac{1}{\tau_m} + \frac{1}{T_{1e}} \quad (\text{A8})$$

The ^{17}O longitudinal relaxation rates in Gd^{3+} solutions are the sum of the contributions of the dipole-dipole (dd) and quadrupolar (q) mechanisms as expressed by Equations (A11-A13) for non-extreme narrowing conditions, where γ_S is the electron and γ_I is the nuclear gyromagnetic ratio ($\gamma_S = 1.76 \times 10^{11} \text{ rad s}^{-1} \text{ T}^{-1}$, $\gamma_I = -3.626 \times 10^7 \text{ rad s}^{-1} \text{ T}^{-1}$), r_{GdO} is the effective distance between the electron charge and the ^{17}O nucleus, I is the nuclear spin (5/2 for ^{17}O), χ is the quadrupolar coupling constant and η is an asymmetry parameter :

$$\frac{1}{T_{1m}} = \frac{1}{T_{1dd}} + \frac{1}{T_{1q}} \quad (\text{A9})$$

with:

$$\frac{1}{T_{1dd}} = \frac{2}{15} \left(\frac{\mu_0}{4\pi}\right)^2 \frac{\hbar^2 \gamma_I^2 \gamma_S^2}{r_{GdO}^6} S(S+1) \times [3J(\omega_I; \tau_{d1}) + 7J(\omega_S; \tau_{d2})] \quad (\text{A10})$$

$$\frac{1}{T_{1q}} = \frac{3\pi^2}{10} \frac{2I+3}{I^2(2I-1)} \chi^2 (1 + \eta^2/3) \times [0.2J_1(\omega_I) + 0.8J_2(\omega_I)] \quad (\text{A11})$$

In Equation (A3) the chemical shift of the bound water molecule, $\Delta\omega_m$, depends on the hyperfine interaction between the Gd^{3+} electron spin and the ^{17}O nucleus and is directly proportional to the scalar

coupling constant, $\frac{A}{\hbar}$, as expressed in Equation (A12).[6]

$$\Delta\omega_m = \frac{g_L \mu_B S(S+1) B}{3k_B T} \frac{A}{\hbar} \quad (\text{A12})$$

The isotopic Landé g factor is equal to 2.0 for the Gd^{3+} , B represents the magnetic field, and k_B is the Boltzmann constant.

The outer-sphere contribution to the chemical shift is assumed to be linearly related to $\Delta\omega_m$ by a constant C_{os} [Equation (A13)]. [7]

$$\Delta\omega_{os} = C_{os} \Delta\omega_m \quad (\text{A13})$$

NMRD

The measured longitudinal proton relaxation rate, $R_1^{obs} = 1/T_1^{obs}$, is the sum of a paramagnetic and a diamagnetic contribution as expressed in Equation (A14), where r_l is the proton relaxivity:

$$R_1^{obs} = R_1^d + R_1^p = R_1^d + r_l [\text{Gd}^{3+}] \quad (\text{A14})$$

The relaxivity can be divided into an inner and an outer sphere term as follows:

$$r_l = r_{lis} + r_{los} \quad (\text{A15})$$

The inner sphere term is given in Equation (A16), where q is the number of inner sphere water molecules. [8]

$$r_{is} = \frac{1}{1000} \times \frac{q}{55.55} \times \frac{1}{T_{lm}^H + \tau_m} \quad (\text{A16})$$

The longitudinal relaxation rate of inner sphere protons, $1/T_{lm}^H$ is expressed by Equation (A11), where r_{GdH} is the effective distance between the electron charge and the ^1H nucleus, ω_I is the proton resonance frequency and ω_S is the Larmor frequency of the Gd^{3+} electron spin.

$$\frac{1}{T_{lm}^H} = \frac{2}{15} \left(\frac{\mu_0}{4\pi} \right)^2 \frac{\hbar^2 \gamma_I^2 \gamma_S^2}{r_{GdH}^6} S(S+1) \times [3J(\omega_I; \tau_{d1}) + 7J(\omega_S; \tau_{d2})] \quad (\text{A17})$$

$$\frac{1}{\tau_{di}} = \frac{1}{\tau_m} + \frac{1}{\tau_{RH}} + \frac{1}{T_{ie}} \quad \text{for } i = 1, 2 \quad (\text{A18})$$

where τ_{RH} is the rotational correlation time of the $\text{Gd-H}_{\text{water}}$ vector.

For small molecular weight chelates (fast rotation), the spectral density function is expressed as in Equation (A19).

$$J(\omega; \tau) = \left(\frac{\tau}{1 + \omega^2 \tau^2} \right) \quad (\text{A19})$$

For slowly rotating species, the spectral density functions are described the Lipari-Szabo approach.[9] In this model we distinguish two statistically independent motions; a rapid local motion with a correlation time τ_l and a slower global motion with a correlation time τ_g . Supposing the global molecular reorientation is isotropic, the relevant spectral density functions are expressed as in Equations (A20-A24), where the general order parameter S^2 describes the degree of spatial restriction of the local motion. If the local motion is isotropic, $S^2 = 0$; if the rotational dynamics is only governed by the global motion, $S^2 = 1$.

$$J(\omega_I; \tau_{d1}) = \left(\frac{S^2 \tau_{d1g}}{1 + \omega_I^2 \tau_{d1g}^2} + \frac{(1 - S^2) \tau_{d1}}{1 + \omega_I^2 \tau_{d1}^2} \right) \quad (\text{A20})$$

$$J(\omega_S; \tau_{d2}) = \left(\frac{S^2 \tau_{d2g}}{1 + \omega_S^2 \tau_{d2g}^2} + \frac{(1 - S^2) \tau_{d2}}{1 + \omega_S^2 \tau_{d2}^2} \right) \quad (\text{A21})$$

$$\frac{I}{\tau_{dig}} = \frac{I}{\tau_m} + \frac{I}{\tau_g} + \frac{I}{T_{ie}} \quad i = 1, 2 \quad (\text{A22})$$

$$\frac{I}{\tau} = \frac{I}{\tau_g} + \frac{I}{\tau_l} \quad (\text{A23})$$

$$J_i(\omega_l) = \left(\frac{S^2 \tau_g}{1 + i^2 \omega_l^2 \tau_g^2} + \frac{(1 - S^2) \tau}{1 + i^2 \omega_l^2 \tau^2} \right) \quad i = 1, 2 \quad (\text{A24})$$

The rotational correlation time, τ_{RH} is assumed to have simple exponential temperature dependence with an E_R activation energy as given in Equation (A25).

$$\tau_{RO} = \tau_{RO}^{298} \exp \left[\frac{E_R}{R} \left(\frac{1}{T} - \frac{1}{298.15} \right) \right] \quad (\text{A25})$$

The outer-sphere contribution can be described by Equations (A26 and A27) where N_A is the Avogadro constant, and J_{os} is its associated spectral density function as given by Equation (A15). [10, 11]

$$\Gamma_{os} = \frac{32 N_A \pi}{405} \left(\frac{\mu_0}{4\pi} \right)^2 \frac{\hbar^2 \gamma_S^2 \gamma_I^2}{a_{GdH} D_{GdH}} S(S+1) [3J_{os}(\omega_l, T_{1e}) + 7J_{os}(\omega_S, T_{2e})] \quad (\text{A26})$$

$$J_{os}(\omega, T_{je}) = \text{Re} \left[\frac{1 + 14 \left(i\omega \tau_{GdH} + \frac{\tau_{GdH}}{T_{je}} \right)^{1/2}}{1 + \left(i\omega \tau_{GdH} + \frac{\tau_{GdH}}{T_{je}} \right)^{1/2} + 49 \left(i\omega \tau_{GdH} + \frac{\tau_{GdH}}{T_{je}} \right) + 19 \left(i\omega \tau_{GdH} + \frac{\tau_{GdH}}{T_{je}} \right)^{3/2}} \right] \quad (\text{A27})$$

$j = 1, 2$

The longitudinal and transverse electronic relaxation rates, $1/T_{1e}$ and $1/T_{2e}$ are expressed by Equation (A28 and A29), where τ_v is the electronic correlation time for the modulation of the zero-field-splitting interaction, E_v the corresponding activation energy and Δ^2 is the mean square zero-field-splitting energy. We assumed a simple exponential dependence of τ_v versus $1/T$ as written in Equation (A30).

$$\left(\frac{1}{T_{1e}}\right)^{ZFS} = \frac{1}{25} \Delta^2 \tau_v \{4S(S+1) - 3\} \left\{ \frac{1}{1 + \omega_s^2 \tau_v^2} + \frac{4}{1 + 4\omega_s^2 \tau_v^2} \right\} \quad (\text{A28})$$

$$\left(\frac{1}{T_{2e}}\right)^{ZFS} = \Delta^2 \tau_v \left(\frac{5.26}{1 + 0.372\omega_s^2 \tau_v^2} + \frac{7.18}{1 + 1.24\omega_s^2 \tau_v^2} \right) \quad (\text{A29})$$

$$\tau_v = \tau_v^{298} \exp \left[\frac{E_v}{R} \left(\frac{1}{T} - \frac{1}{298.15} \right) \right] \quad (\text{A30})$$

The diffusion coefficient for the diffusion of a water proton away from a Gd^{3+} complex, D_{GdH} , is assumed to obey an exponential law versus the inverse of the temperature, with activation energy E_{DGdH} , as given in Equation (A31). D_{GdH}^{298} is the diffusion coefficient at 298.15K.

$$D_{GdH} = D_{GdH}^{298} \exp \left\{ \frac{E_{GdH}}{R} \left(\frac{1}{298.15} - \frac{1}{T} \right) \right\} \quad (\text{A31})$$

References:

1. C. Wang, S. D. Wettig, M. Foldvari, R. E. Verrall, *Langmuir*, 2007, **23**, 8995.
2. P. Carpena, J. Aguiar, P. Bernaola-Galván, C. Carnero Ruiz, *Langmuir*, 2002, **18**, 6054.
3. Swift TJ, Connick RE, *J Chem Phys*, 1962, **37**, 307.
4. Zimmerman JR, Brittin WE, *J Phys Chem*, 1957, **61**, 1328.
5. Micskei K, Helm L, Brucher E, Merbach AE, *Inorg Chem*, 1993, **32**, 3844.
6. Brittain HG, Desreux JF, *Inorg Chem*, 1984, **23**, 4459.
7. Gonzalez G, Powell DH, Tissieres V, Merbach AE, *J Phys Chem*, 1994, **98**, 53.
8. Luz Z, Meiboom S, *J Chem Phys*, 1964, **40**, 2686.
9. Dunand FA, Tóth E, Hollister R, Merbach AE, *J Biol Inorg Chem*, 2001, **6**, 247.
10. Freed JH, *J Chem Phys*, 1978, **68**, 4034.
11. Koenig SH, Brown RD, Spiller M, et al, *Biophys J*, 1992, **61**, 776.